

Optimization of Free Piston Expander Based Organic Rankine Cycle

Dimpykumari Anilbhai Patel

A thesis
in
The Department
of
Mechanical, Industrial and Aerospace Engineering

Presented in Partial Fulfillment of the Requirements
for the Degree of
Masters of Applied Science (Mechanical Engineering)
Concordia University
Montréal, Québec, Canada

December 2021
© Dimpykumari Anilbhai Patel, 2021

CONCORDIA UNIVERSITY

School of Graduate Studies

This is to certify that the thesis prepared

By: Dimpykumari Anilbhai Patel

Entitled: “Optimization of Free Piston Expander Based Organic Rankine Cycle”

and submitted in partial fulfillment of the requirements for the degree of

Master of Applied Science (Mechanical Engineering)

complies with the regulations of the University and meets the accepted standards with respect to originality and quality.

Signed by the final examining committee:

_____ Chair & Examiner
Dr. Carole El Ayoubi

_____ Examiner
Dr. Lyes Kadem

_____ Thesis Supervisor
Dr. Charles Basenga Kiyanda

Approved by _____
Dr. Sivakumar Narayanswamy, MASc Program Director
Department of Mechanical, Industrial and Aerospace Engineering

Dr. Mourad Debbabi, Associate Dean, Research and Graduate Studies
Gina Cody School of Engineering and Computer Science

Abstract

Optimization of Free Piston Expander based Organic Rankine Cycle

Dimpykumari Anilbhai Patel

Thanks to its simple design, operational flexibility and potentially higher thermal efficiency at higher pressure ratios, the free piston expander (FPE) is gaining popularity and attention from researchers. A lot of work is expanded to implement the FPE concept in the organic Rankine cycle (ORC) for waste heat recovery. However, steady-state models that predict the efficiency and power output of FPEs under varying conditions are not available. The main objective of this work is to build a steady-state model to optimize the FPE-based, waste heat recovery cycle using a suitable working fluid. A thermodynamic analysis is carried out to match the unsteadiness of the FPE with the steady heat rejection, pressurization, and heat recovery of the ORC. Entropy before condensation and internal energy after constant volume filling is optimized, keeping the thermodynamic state of the fluid coming out of the heat exchanger fixed on the saturated vapor line. From optimized values, work output and efficiency for a specified condition (hot and cold source temperatures) are calculated. Targeted power output, maximum allowable piston velocity, and frequency are constrained by the system, from which the sizing of an FPE is derived. The sizing criteria provides a mean for the selection of the optimum working fluid. The analytical results show that the efficiency increases with the increasing expansion ratio up to a certain value, but however has a negative effect on specific power. Increasing the initial volume, before the filling of the FPE takes place, decreases both the efficiency and specific power and should be minimized for optimal operation. Optimum fluid selection is also carried out for two test cases with varying hot source temperatures and maximum piston velocity.

Acknowledgment

I would wholeheartedly like to thank a few people, who helped me in all possible manners towards the completion of my master's degree. First, I would like to express my sincere gratitude and immense respect to my research supervisor Dr. Charles Basenga Kiyanda for trusting me and giving me this opportunity. Without his persistent guidance and patience, it would never be possible for me to complete this thesis “Optimization of Free Piston Expander Based Organic Rankine Cycle”. After that, my special thanks go to “Novopower International Inc.” and “Mitacs Accelerate” for providing me with this project topic and funding, without which my thesis work and MASc journey would not have started. I would also like to acknowledge the staff at Novopower, Philip Raphals, Joris Naudin, and Tamas Bertenyi for their assistance during the project. Before and during my studies at Concordia University, my parents, Anilbhai and Bhartiben, grandmother Valiben, brother Fenil, my bachelors' supervisor/mentor Dr. Digvijay Kulshreshtha and his family members Shruti, Angel, Aahna, and Nisarg supported and helped me to stay motivated from overseas. I also appreciate my colleagues, who helped me during this journey.

Table of Content

List of Figures	VII
List of Tables.....	VIII
List of Acronyms.....	IX
Nomenclature	X
List of Subscripts.....	XII
1 Introduction.....	1
1.1 Objective and Motivation	2
2 Literature Review	4
2.1 Thermodynamic Cycles.....	4
2.1.1 Basic Rankine Cycle	4
2.1.2 Kalina Cycle	4
2.1.3 Organic Rankine Cycle	5
2.1.4 Tri-Lateral Cycle (TLC).....	6
2.2 Types of Expanders	7
2.2.1 Turbo-expander	7
2.2.1.1 Axial Flow Turbine	7
2.2.1.2 Radial Inflow Turbine (RIT)	7
2.2.1.3 Radial Outflow Turbine (ROT)	8
2.2.2 Scroll Expander	8
2.2.3 Screw Expander.....	9
2.2.4 Reciprocating Piston	10
2.2.5 Free-Piston Expander	10
2.3 Review of Working Fluid Selection Strategies	11
2.4 Review of Free Piston Expander Cycles	17
2.4.1 Existing FPE Implementations.....	17
2.4.2 Efficiency and Performance Predictions and Calculations	17
3 Matched Steady-Unsteady Thermodynamic Cycle Analysis	19
3.1 Overview of Cycle Processes.....	19
3.2 Steady Processes	20
3.3 Unsteady Processes	21
3.3.1 State Determination.....	21
3.4 Specific Work Output and Efficiency	24
3.5 Length and Time Scale Calculations.....	25
3.5.1 Targeted Power and Piston Diameter	25
3.5.2 Cycle Time	25
4 Result and Analysis	27
4.1 Impact of Expansion Ratio, r_p	27
4.2 Impact of Fill Ratio, r_f	27
4.3 Impact of r_f and r_p on Specific Power	33
4.4 Dependence on Hot and Cold Source Temperatures	36
5 Case Study for Fluid Selection	41
5.1 Case 1 and 1b	41
5.2 Case 2 and 2b	42
6 Conclusion and Future Work.....	44
7 Bibliography	45
Appendix A: T - s curves for the fluids Novec649 and R1234yf.....	48
Appendix B: Specific power vs. efficiency plots for all fluids considered in the case study ..	49

Appendix C: Possible fluids for the case studies	51
Appendix D: Matched steady-unsteady algorithm. Pseudocode.....	63

List of Figures

Figure 1: Worldwide fossil fuel consumption from the year 1965 to 2020 [1].....	1
Figure 2: Simple ideal Rankine cycle and $T - s$ diagram [17].....	4
Figure 3: Flow diagram of simple Kalina cycle [18].....	5
Figure 4: Schematic of ORC and $T - s$ diagram [20].....	6
Figure 5: Schematic of TLC and $T - s$ diagram [21].....	6
Figure 6: Schematic of axial flow turbine [11].....	7
Figure 7: Meridional scheme (left) and RIT (right) [22].....	8
Figure 8: Schematic of ROT [11].....	8
Figure 9: Principle of Scroll expander [23].....	9
Figure 10: Scroll Expander [24].....	9
Figure 11: Schematic of twin-screw expander/screw expander [11].....	9
Figure 12: Working of reciprocating piston expander [26].....	10
Figure 13: Structure of free-piston linear expander (FPLE) [27].....	10
Figure 14: Typical T-s diagram of wet, isentropic, and dry fluids. Classification is based on the slope of the vapor curve [28].....	11
Figure 15: T-s diagram for the ORC for (a) pure cyclohexane and (b) zeotropic mixture of cyclohexane and R123 [15].....	14
Figure 16: Effect of vaporization heat on the irreversibility in the heat transfer process [13].....	15
Figure 17: Efficiency and output power dependency on piston mass [46]. Note the efficiency is wrongly reported to be a percentage and is instead in decimal form....	18
Figure 18: Operating frequency dependency on piston mass for fixed input heat $E = 10\text{mJ/cycle}$ and load $b = 1\text{Ns/m}$ [46].....	18
Figure 19: Piston displacement [double acting FPE].....	19
Figure 20: $T-s$ and $P-v$ diagram.....	20
Figure 21: Adiabatic filling process of working fluid at constant volume.....	22
Figure 22: Adiabatic filling process of working fluid at constant pressure.....	23
Figure 23: Variation in efficiency with expansion ratio for a given $r_f = 0.1$. The incomplete line for toluene is due to the failure of Brent's method.....	27
Figure 24: Variation in efficiency with fill ratio for a given $r_p = 2$	28
Figure 25: Variation in temperatures (at points p, a, b and c) with fill ratio, at $r_p = 2$ for R1234yf.....	29
Figure 26: Variation in temperatures (at points p, a, b and c) with fill ratio, at $r_p = 2$ for novoc649.....	29
Figure 27: Variation in temperatures (at points p, a, b and c) with fill ratio, at $r_p = 2$ for toluene.....	30
Figure 28: Variation in temperatures (at points p, a, b and c) with fill ratio, at $r_p = 2$ for water.....	30
Figure 29: Increase in the area for condenser work under $T-s$ diagram.....	31
Figure 30: Variation in temperatures (at points p, a, b and c) with fill ratio, at $r_p = 4$ for water.....	31
Figure 31: Variation in maximum expansion ratio achieved with fill ratio.....	32
Figure 32: $T - s$ curve, Water.....	32
Figure 33: $T - s$ curve, Toluene.....	33
Figure 34: Variation of specific power with expansion ratio at $r_f = 0.1$. The incomplete line for toluene is due to the failure of Brent's method.....	33
Figure 35: Variation in specific power and Efficiency at $r_f = 0.1$. The incomplete line for toluene is due to the failure of Brent's method.....	34

Figure 36: Variation in specific power with expansion ratio for R1234yf at different r_f .	35
Figure 37: Variation in zeta with $r_p / r_{p,max}$. The incomplete line for toluene is due to the failure of Brent's method.	35
Figure 38: Variation in zeta with $r_p / r_{p,max}$ at different r_f for R1234yf.	36
Figure 39: Efficiency vs. hot source temperature at given cold source temperature of 293K at $r_p = 2$.	36
Figure 40: Efficiency vs. hot source temperature at given cold source temperature of 293K at $r_p = 4$.	37
Figure 41: Variation in efficiency with hot source temperature at r_p of 2, 4 and $r_{p,max}$ for R1234yf.	37
Figure 42: Efficiency vs. hot source temperature at given cold source temperature of 293K at $r_p = r_{p,max}$. The incomplete line for toluene is due to the failure of Brent's method.	38
Figure 43: Variation in maximum expansion ratio with a hot source temperature.	38
Figure 44: Efficiency vs. cold source temperature at a given hot source temperature of 348K and $r_p = 2$.	39
Figure 45: Variation in efficiency with cold source temperature at r_p of 2, 4 and $r_{p,max}$ for R1234yf.	39
Figure 46: Efficiency vs. cold source temperature at given hot source temperature of 348K at $r_p = r_{p,max}$. The incomplete line for toluene is due to the failure of Brent's method.	40
Figure 47: Specific power vs. efficiency curve for fluid selection.	42
Figure 48: $T-s$ curve, Novec649.	48
Figure 49: $T-s$ curve, R1234yf.	48
Figure 50: P_{sp} vs. efficiency at different expansion ratios for all fluids in COOLPROP for case 1.	49
Figure 51: P_{sp} vs. efficiency at different expansion ratios for all fluids in COOLPROP for case 1b.	49
Figure 52: P_{sp} vs. efficiency at different expansion ratios for all fluids in COOLPROP for case 2.	50
Figure 53: P_{sp} vs. efficiency at different expansion ratios for all fluids in COOLPROP for case 2b.	50
Figure 54: Flowchart to calculate all required parameters for a single fluid based on a given constraint.	63

List of Tables

Table 1: Examples of dry, wet and isentropic fluids.	12
Table 2: Phase-out schedule of ODS as per Montreal Protocol [33].	13
Table 3: Set of conditions for case study.	41
Table 4: Fluid list and corresponding parameters for case 1; ODP & GWP data [47].	54
Table 5: Fluid list and corresponding parameters for case 1b; ODP & GWP data [47].	59
Table 6: Fluid list and corresponding parameters for case 2; ODP & GWP data [47].	60
Table 7: Fluid list and corresponding parameters for case 2b; ODP & GWP data [47].	62

List of Acronyms

ALT	Atmospheric Lifetime
BDC	Bottom Dead Centre
CFCs	Chlorofluorocarbons
EES	Engineering Equation Solver
EOS	Equation of State
FOM	Figure of Merit
FPE	Free Piston Expander
FPE-LG	Free Piston Expander Linear Generator
FPLE	Free Piston Linear Expander
GHG	Green House Gases
GWP	Global Warming Potential
HCFCs	Hydrochlorofluorocarbons
HFCs	Hydrofluorocarbons
ICEs	Internal Combustion Engines
LG	Linear Generator
ODP	Ozone Depletion Potential
ODS	Ozone Depleting Substances
OMR	Optimal Mixture Ratio
OET	Optimal Evaporation Temperature
ORC	Organic Rankine Cycle
RIT	Radial Inflow Turbine
ROT	Radial Outflow Turbine
TDC	Top Dead Centre
TLC	Trilateral Cycle
WF	Working Fluid

Nomenclature

A_P	Piston area	m^2
C_p	Average specific heat	$kJ/kg.K$
dT	Temperature difference between evaporation and condensation	K
E	Total energy	J
f	Frequency	Hz
h	Enthalpy	J/kg
H_v	Vaporization latent heat	kJ/kg
Ja	Jacob number	Dimensionless
L_B	Length of FPE till which cylinder is being filled with WF	m
L_b	Latent heat	kJ/kg
L_C	Length of FPE till which WF is being expanded	m
L_O	Clearance length	m
L_{Total}	Total length of the double acting FPE cylinder	m
\dot{m}	Mass flow rate	kg/sec
$m_{dP=0}$	Mass injected at constant pressure	kg
$m_{dV=0}$	Mass injected at constant volume	kg
m_{inj}	Total mass injected per cycle	kg
N	Exponent of working fluid	Dimensionless
P_B	Boiler pressure	kPa
P_C	Condenser pressure	kPa
P_{evap}	Evaporation pressure	kPa
$P_{expanded}$	Expansion pressure	kPa
P_{target}	Targeted power	watt
\dot{Q}	Net heat transfer	J/sec
R	Universal gas constant	$kJ/ mol. K$
r_f	Fill ratio	Dimensionless
r_P	Expansion ratio	Dimensionless
s	Specific entropy	$J/kg K$
T_b	Normal boiling point	K
T_{cr}	Critical temperature	K
T_{cold}	Cold source temperature	K
T_{cond}	Condensation temperature	K
T_{evap}	Evaporation temperature	K

T_{hot}	Hot source temperature	K
U	Internal energy	J
u	Specific internal energy	J/kg
V	Volume	m^3
v	Specific volume	m^3/kg
v_p	Piston velocity	m/sec
$v_{p,\text{fill}}$	Velocity at which cylinder is being filled	m/sec
$v_{p,\text{max}}$	Maximum piston velocity	m/sec
\dot{W}	Net work done	J/sec
x	Displacement of piston	m
ρ	Density	kg/m^3
τ	Total cycle time	sec
τ_{exp}	Total expansion time	Dimensionless
τ_{fill}	Total injection time	Dimensionless

List of Subscripts

f	Final state
i	Initial state
1	State 1, pump inlet
2	State 2, heat exchanger inlet
3a	State 3a, after constant volume fluid injection
3b	State 3b, before expansion (after constant pressure fluid injection)
3c	State 3c, after expansion
3p	State 3p, heat exchanger outlet
4	State 4, condenser inlet

1 Introduction

In man-made facilities (industrial, vehicular and commercial) energy demand is increasing day by day. It mostly depends on fossil fuels, due to which, fossil fuel consumption is increasing rapidly [1]. The worldwide fossil fuel consumption trend over the past few years is shown in figure 1. To fulfill this increasing energy demand, excessive drilling of fossil fuels carried out over the past years resulted in their ongoing depletion. It is predicted that by the end of the 21st century, the world will be running out of all fossil fuels [2]. On the other hand, in power plants and vehicles, only 30-40% of fuel's combustion energy is used to obtain work, a few percentage energies are used for cooling, convective, and radiative heat transfer. About 30-40% of energy is being wasted through exhaust [3] and contributing to pollution, greenhouse gas (GHG) emissions, and related problems such as global warming, climate change, sea-level rise, etc. It can be summarized as, "The fuel resources are being used excessively, with a lot of energy wastage, additionally harming the environment and living beings in all possible ways".

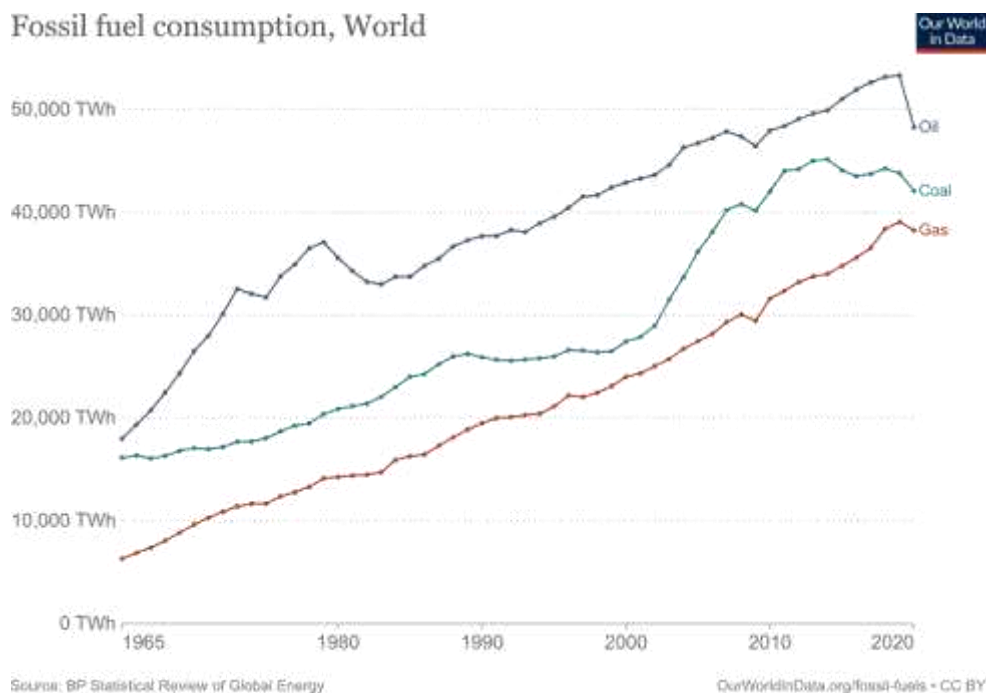


Figure 1: Worldwide fossil fuel consumption from the year 1965 to 2020 [1]

To these problems, one possible solution is to recapture and reuse the waste heat. Upon waste heat utilization, use of traditional fuel and emission from the facility can be lowered. Waste heat utilization can be done in two ways: cogeneration and power generation. Cogeneration is using the waste heat from the exhaust to heat/boil water for cooling/heating load requirements [4]. Cogeneration is limited by distance. If plants are far away from the facility where it is to be used, then hot water/steam on the arrival at the facility has already lost potential for output. Power generation using waste heat boilers and steam turbines, from the industrial waste heat is another way to recapture energy. For low-temperature applications, the power conversion efficiency is poor, and the cost associated is high [5]. Hence, there is a requirement of designing a more efficient and versatile system for waste heat recovery (WHR). Moreover, governments of different nations are taking steps, by implementing certain norms, such as prescribed level of emission, waste disposal techniques, recycling of the materials, etc., that must be followed by any industry, to continue operation. It is challenging to reduce emissions from the plants and simultaneously achieve maximum possible efficiency with minimal cost. Much research has been carried out to achieve maximum efficiency [6] through WHR and is ongoing.

The Rankine cycle has been used for waste heat recovery for decades. To extract more out of waste heat, research is tackling optimization of Rankine cycle for higher efficiency by introducing modified cycles such as ORC, Kalina cycle (KC), etc. ORC uses an organic working fluid whose boiling point is lower than that of water, whereas the Kalina cycle most often uses an NH₃-Water mixture. Both ORC and Kalina cycles work with a lower temperature range. Mixtures of a working fluid in the Kalina cycle give a variable evaporation temperature, which results in lower irreversibility. However, the simple configuration, high reliability, and lower maintenance requirements of ORC make such cycles more attractive in many situations [7] [8].

The efficiency of the ORC system is highly dependent on the expansion device [8]. According to the application requirements, it is mandatory to choose the best-suited expansion device considering several parameters such as isentropic efficiency, power output, pressure ratio, rotational speed, lubrication requirements, weight, reliability, availability, dynamic balance, size, cost [9], and off-design performance [10]. Generally, expansion devices are of two types: turbo-expanders and volumetric expansion machines. Turbo-expanders are used for medium to large scale applications because of their high efficiency, whereas volumetric expansion machines such as piston, scroll, and screw expanders are best suited for smaller power outputs [11] because of the low rotational speed, small flow rates over a high-pressure ratios and ability to handle two-phase fluid [12]. In volumetric expanders such as piston expanders, fluid is filled in a fixed volume, displacement of this fluid takes place, and then it discharges from the cylinder, causing the fluid movement not to be continuous [11].

With the expansion device to be used, the efficiency of an ORC also depends on the working fluid, which in turn depends on the heat source and pressure ranges [13]. One or few working fluids can give optimum results for a specific case, which can be obtained considering various aspects, such as thermal efficiency, exergy loss [3], power output, total heat capacity, expander size [14], type of fluid (dry, wet, isentropic) [15] [16], and effect on the environment. More complex fluids such as zeotropic mixtures, if used as a working fluid, give non-isothermal phase change, increasing efficiency and power output [12]. Creating new mixtures can further help in optimizing cycle efficiency.

Turbo expanders are generally used for large power applications where flow rates are high. Volumetric expanders-screw, scroll, and piston are suitable for small-scale applications but impose limitations due to their complex design. Simple design, operational flexibility, and potentially higher thermal efficiency at higher pressure ratios of the free piston expander (FPE) make it suitable for WHR at low temperatures.

1.1 Objective and Motivation

Novopower International Inc. provides solutions to recycle waste heat into useful power, using free-piston ORC generators. This company is an industrial partner financing this work and benefiting from the science and technology developed here. The main driver for this industrial partner's interest in the FPE is its versatility and range of off-design operations.

The company has developed a time-resolved model, with losses. By definition, a complete run of the model, from startup, until the asymptotic steady-state operation, must be carried out for every candidate working fluid, geometry, etc.

There is therefore a need for a model to more rapidly explore the space of possible geometric size and working fluids, subject to size constraints and power requirements.

The main objective of this work is to build this steady-state model to optimize the FPE-based, waste heat recovery cycle using a suitable working fluid.

Chapter 2 provides information about the possible thermodynamic cycle configurations for WHR and types of expanders, their advantages and disadvantages, which can be helpful for the selection of expanders according to the application demand. A detailed description of the fluid selection procedure is also discussed. Existing FPE implementations and performance predictions are also reviewed. In chapter 3, analysis to match the steady and unsteady part of the cycle is carried out and sizing of the FPE is derived. Chapter 4 contains results from the analysis carried out to study the impact of expansion ratio and fill ratio on efficiency, the relation between specific power and efficiency, the effect of hot and cold source temperature on efficiency, and possible expansion ratios. In chapter 5, two source temperatures are examined for 4 different sets of conditions and their results are presented. Chapter 6 concludes the work done and poses the ideas for future work.

2 Literature Review

2.1 Thermodynamic Cycles

Various available thermodynamic cycles for WHR, are discussed below. The analysis of the cycle efficiency and performance varies according to the details of the implementation.

2.1.1 Basic Rankine Cycle

The Carnot cycle model gives the highest efficiency of all cycles, but it is not adaptable in practice because it requires isothermal heat addition and isothermal condensation. These two operations in the Carnot cycle can be replaced by isobaric heat addition and isobaric condensation, to achieve the Rankine cycle, which is more practical. The Rankine cycle is ideal for power plants [17]. Water is used as a working fluid. Saturated liquid at state 1 is pumped to the boiler (state 2), where it changes the phase and superheated to temperature T_3 at constant pressure P_2 . Superheated steam enters the turbine, expands to state 4, producing shaft work. It rejects heat in the condenser and enters the boiler again through the pump. The efficiency of the Rankine cycle can be increased by implementing several modifications to the cycle such as lowering condenser pressure, increasing boiler pressure, super-heating the steam to high temperature, reheating, and regeneration using a feedwater heater [17].

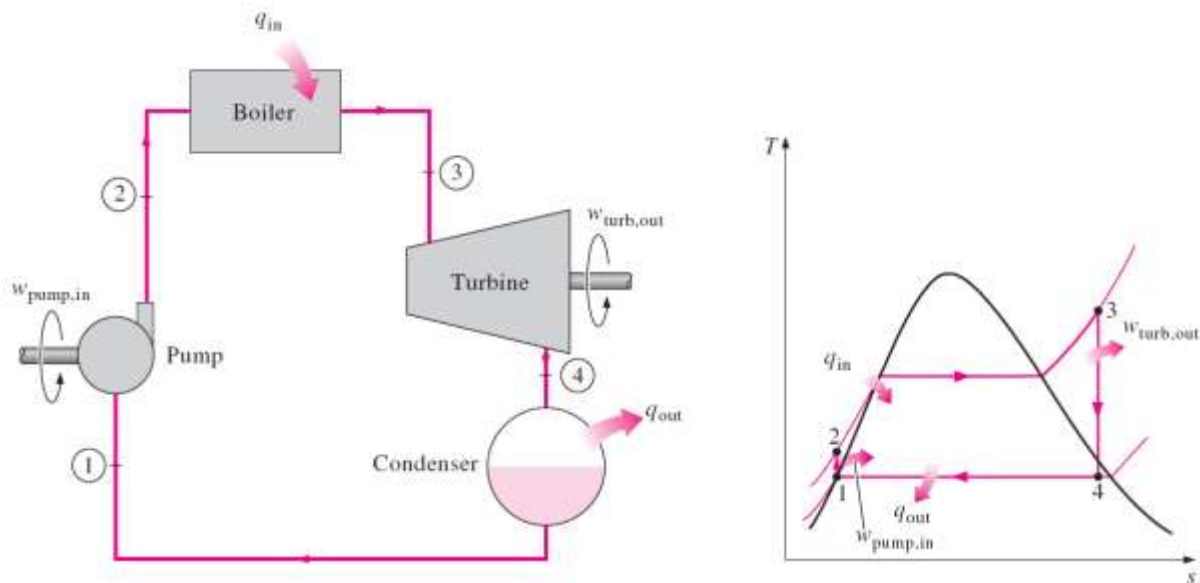


Figure 2: Simple ideal Rankine cycle and $T-s$ diagram [17]

2.1.2 Kalina Cycle

Alexander I. Kalina proposed a new and more efficient cycle that uses a water-ammonia mixture as a working fluid to replace the traditional steam Rankine cycle [18]. Figure 3 shows the basic configuration of the Kalina cycle (modified Rankine cycle) as bottoming cycle, where numbers in the squared bracket stand for the devices of the cycle (details below the figure) and numbers without bracket indicates the state points. Exhaust gases (1,2) from the main cycle (topping cycle) enters the boiler, heat the ammonia-water mixture. Superheated mixture (3) then enters the turbine and expands to state (5), producing work output (4). This mixture then gets cooled (6,7,8), passing through Distiller, Reheater1, and Reheater2. Less concentrated liquid (Ammonia poor) is then added (9,10) to the mainstream. It gets condensed (11) in the absorber (12,13), compressed (14) with the help of a condensate pump, and enters the separator after

being heated up (15,16,17,18). From the separator, less concentrated fluid (19) gets cooled (20,21) and decompressed in throttle (9), whereas Ammonia rich vapor (22) is cooled (23), some fresh mixture is added (24) at this stage to reduce the ammonia concentration up to 70% (25). It cools down (26) again, condensed (27), compressed (30), and fed to the boiler via a Feedwater heater (31). Ammonia-water mixture as working fluid gives varying boiling and condensing temperature, thus reducing losses in the heat transfer process, simultaneously it presents the risk of explosion as ammonia is highly flammable.

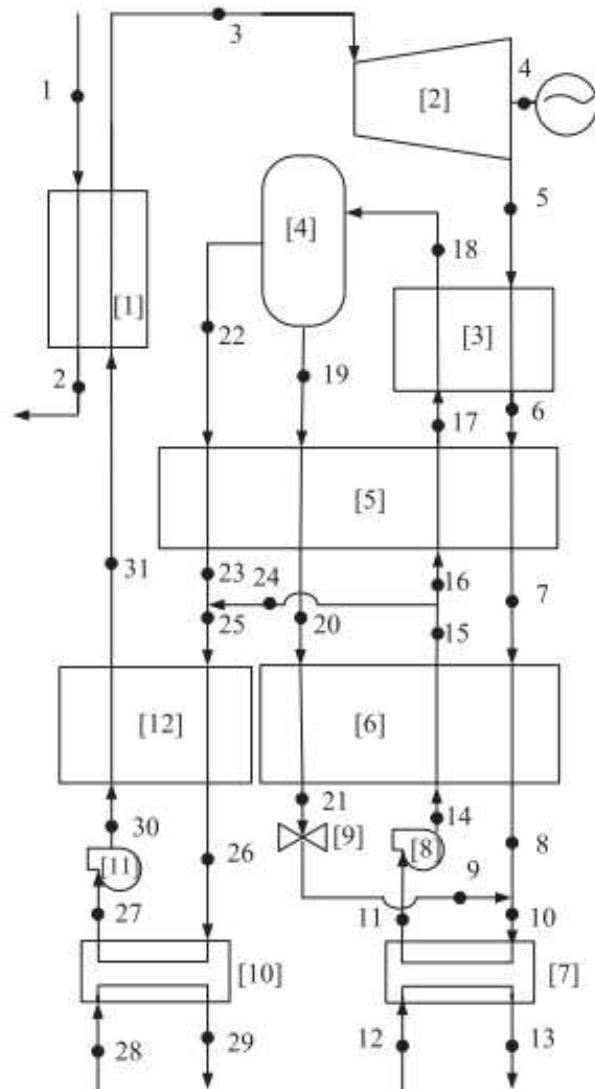


Figure 3: Flow diagram of simple Kalina cycle [18]

Note: [1] Boiler, [2] Turbine, [3] Distiller, [4] Separator, [5] Reheater1, [6] Reheater2, [7] Absorber, [8] condensate pump, [9] Throttle, [10] Condenser, [11] Boiler feed pump, [12] Feed water heater

2.1.3 Organic Rankine Cycle

ORC is a modification of the Rankine cycle, consisting of using organic fluids with lower boiling temperatures as working fluid rather than water. As an ORC uses a heavy molecular weight organic fluid, it is suitable for medium to small-scale applications. It can efficiently recover heat from low-temperature waste heat sources and is famous because of its simple design [19]. Organic fluid at state 1 (T_1, P_1) is pumped to the evaporator (T_2, P_2), where it gets

heated to a temperature (T_3) lower than the critical point temperature. The heating process is ideally isobaric. The vapor leaving the evaporator enters the expander and expands isentropically to state 4 ($T_4, P_4=P_1$), producing work. After expansion, the working fluid is condensed (T_1, P_1) and fed back to the evaporator via a pump [20].

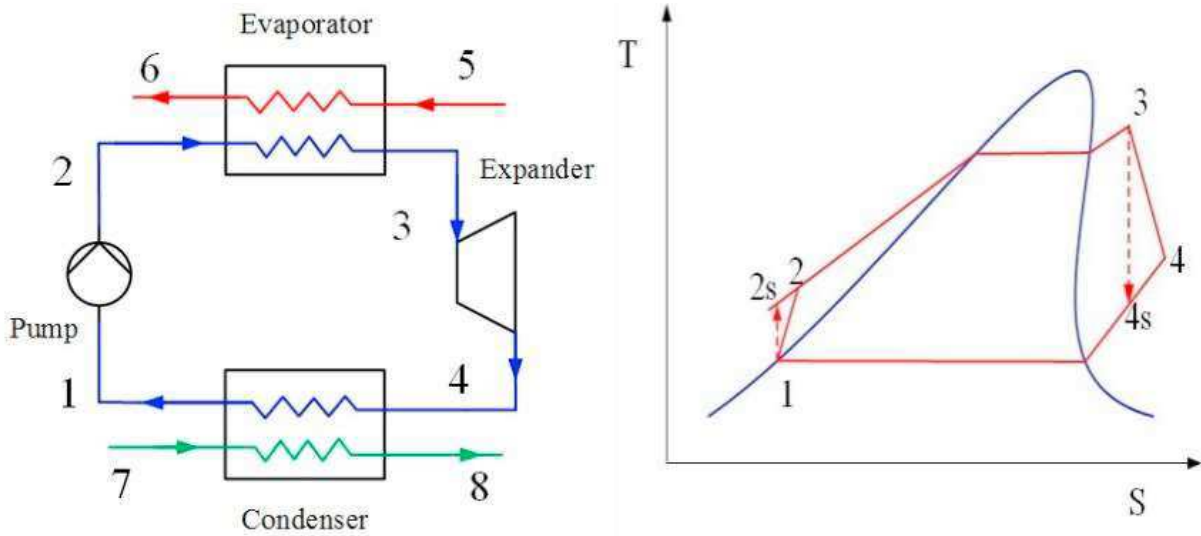


Figure 4: Schematic of ORC and $T-s$ diagram [20]

2.1.4 Tri-Lateral Cycle (TLC)

TLC system encompasses pump, heat exchanger, expander, and condenser. In TLC, unlike the Rankine cycle, the saturated liquid is being expanded [21]. Saturated liquid at temperature T_1 and pressure P_1 is pumped to pressure P_2 , enters heat exchanger, where it gets heated to the boiling point temperature T_3 at constant pressure P_2 . After that it expands into a two-phase mixture at state 4, producing work, gets condensed to state 1, and the cycle keeps going [20]. In this cycle, expander selection is crucial as it should be able to handle two-phase expansion. TLC is the most promising WHR technology among all, because of its high heat transfer capability. TLCs are still in the stage of technical development; hence ORCs are widely used for WHR despite its exergy destruction flow due to temperature mismatching [20].

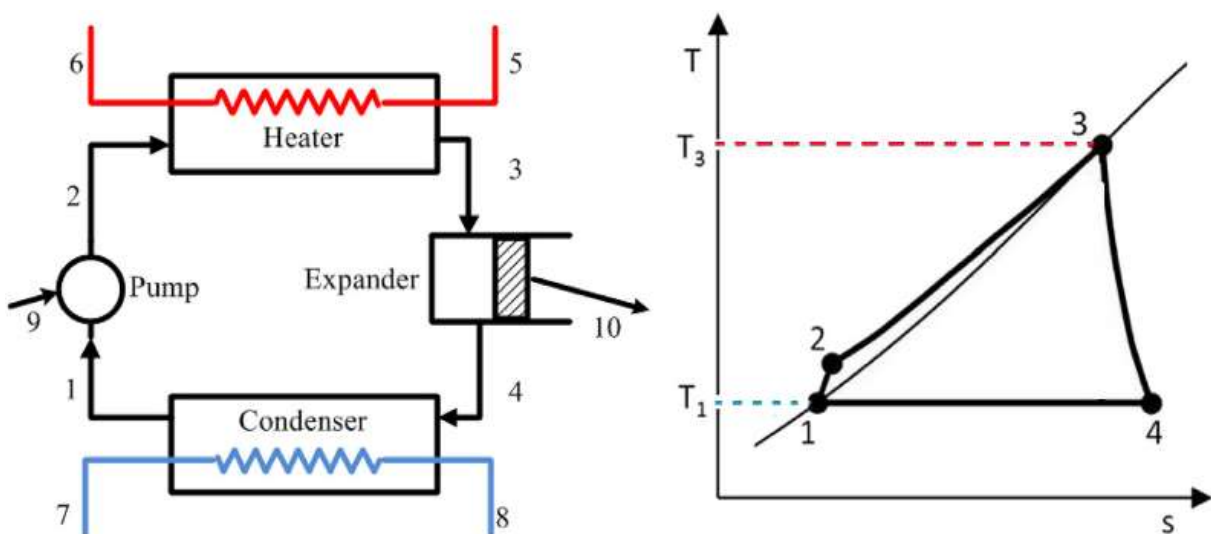


Figure 5: Schematic of TLC and $T-s$ diagram [21]

2.2 Types of Expanders

Several different types of expanders are used for different applications and can be coupled to the number of variations on the Rankine cycle. The analysis of their underlying cycles and efficiency may differ slightly. Types of available expanders and their characteristics are explained below.

2.2.1 Turbo-expander

In the turboexpanders, high pressurized fluid from the evaporator enters into the turbine via a nozzle, which converts the fluid's static pressure into a high flow velocity. This high-velocity fluid passes through the series of blades mounted on a shaft, giving away momentum. Mechanical energy from the shaft is then converted into electrical energy through the generator [11]. Turbo expanders, due to their flexibility, scalability, and higher efficiency have several configurations (impulse and partial admission machine, reaction radial machine, reaction axial machine, multistage axial, etc.) and are used in many applications according to the operational conditions [11] [22]. For organic fluids, turbine design is a bit complicated (may require converging-diverging blades) as they have a lower speed of sound, which results in a supersonic/transonic flow promoting shock formation, choked flow, and losses [11] [22] in the expander. ORC can be built using both the axial and radial type turbines, described below.

2.2.1.1 Axial Flow Turbine

In this type of expander, the working fluid flows in a parallel direction to the shaft [22]. For small-scale ORC applications, while designing an axial flow turbine, blade dimensions come out to be tiny for smaller mass flow rates, which is not capable of handling tip clearance, causing the efficiency to drop significantly [11]. Generally, axial flow turbines are used where flow rates are high with 2 or 3 stages. (large scale applications - power plants with megawatt-scale output power) [22].

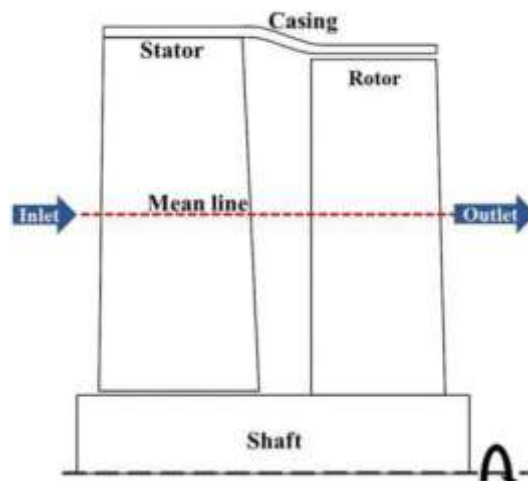


Figure 6: Schematic of axial flow turbine [11]

2.2.1.2 Radial Inflow Turbine (RIT)

The high-pressure working fluid breaks into the casing radially, changes direction tangentially around the rotor inlet, and exits axially. RIT can work with small flow rates as blade profile is less sensitive to flow rates, unlike the axial flow turbines. RIT can handle dense organic fluids because of its robust design. As radius decreases from the rotor inlet to exit, single-stage expansion is possible. The main disadvantage of this configuration is that both the blades and

disc are subjected to heat, however, ORC operates in a low-temperature range, and hence this disadvantage can be easily overcome [11].

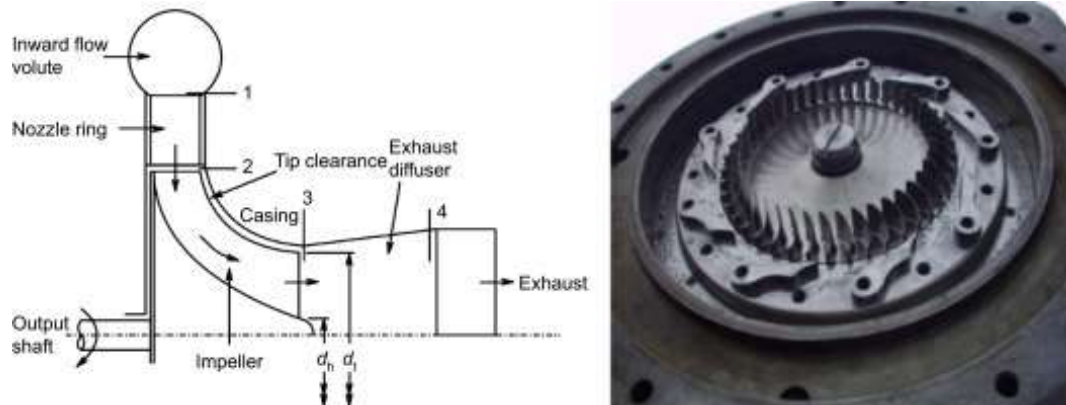


Figure 7: Meridional scheme (left) and RIT (right) [22]

2.2.1.3 Radial Outflow Turbine (ROT)

In ROT, the fluid enters axially at the axis of rotation and moves outward radially. Because of the large area at the exit, losses can be reduced simultaneously as flowing fluid stays in contact with a larger surface area, reducing its efficiency compared to RIT [11].

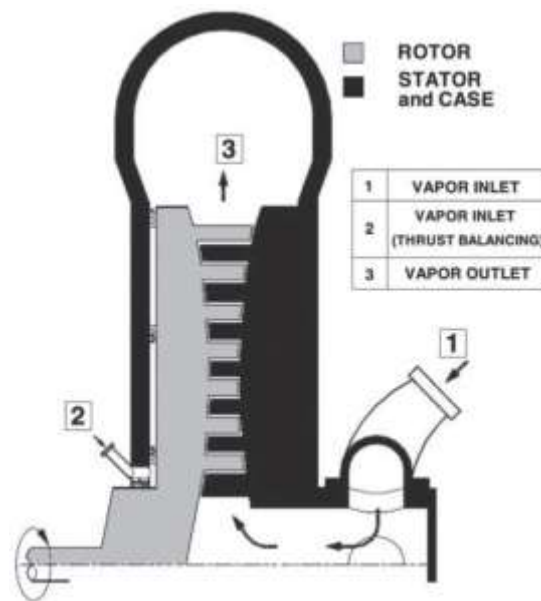


Figure 8: Schematic of ROT [11]

2.2.2 Scroll Expander

A scroll expander comprises two spirals: orbiting scroll and fixed scroll [11]. The orbiting scroll moves radially across the fixed scroll, which can move axially [23]. An anticlockwise orbiting movement gives an expander effect, whereas the opposite movement makes it a compressor [23]. Initially, a volume of working fluid gets trapped at the center and subsequently moves outward. This volume of the fluid expands in the chamber and leaves the expander via a discharge port [23]. As it has a discharge port, it does not require an exhaust valve, thus reducing the noise of operation. The volumetric ratio is limited to 1.5-5 [11], putting a limit on the usable pressure ratio [10]. Two expanders in series can be used to increase the volume ratio. These types of expander can handle large amounts of liquid [10] and low flow rates [23], and hence are used for low power output applications up to several (10-12) kW [11].

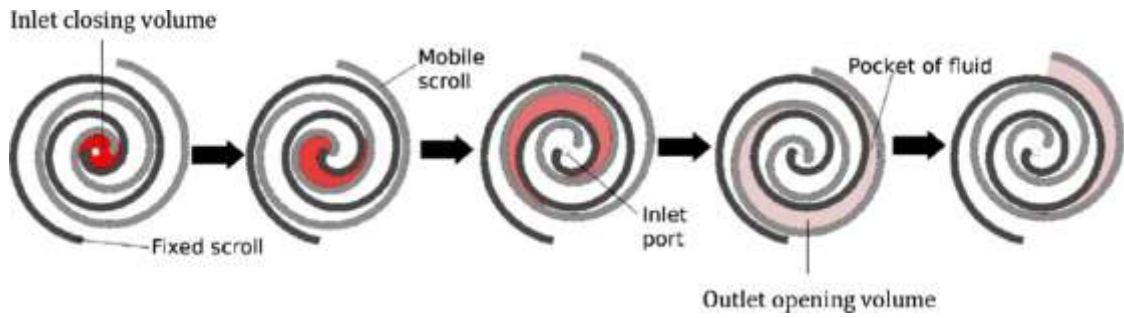


Figure 9: Principle of Scroll expander [23]



Figure 10: Scroll Expander [24]

2.2.3 Screw Expander

This design consists of two helical rotors (male and female), meshed into each other creating small volumes to trap and expand the working fluid. Two rotors engage directly, creating wear and tear due to friction. Hence lubrication is required, which also helps sealing clearance and reduce leakage losses. The allowable volumetric ratio is between 2 and 8. This type of expander can be used where power requirement varies from several kW to 1MW. Isentropic efficiencies can reach up to 70% [11].

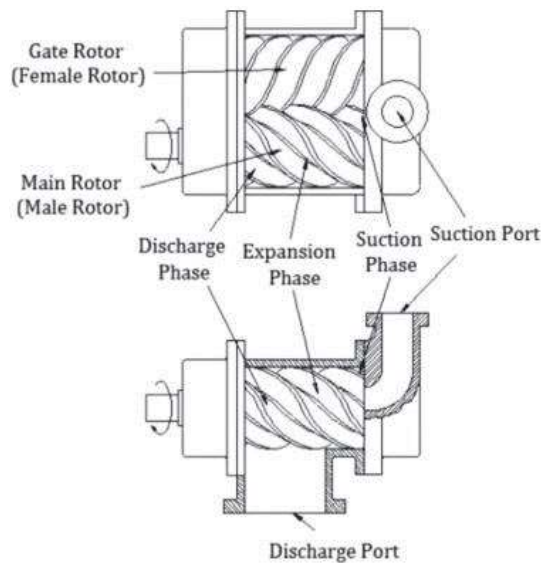


Figure 11: Schematic of twin-screw expander/screw expander [11]

2.2.4 Reciprocating Piston

In a reciprocating piston expander, when the piston is at the top dead center (TDC), working fluid accumulates the cylinder through the inlet valve. After that, inlet valve gets closed. Working fluid expands in the cylinder, pushing the piston down towards the bottom dead center (BDC), giving away energy to the crankshaft through the connecting rod. Then, the exhaust valve opens and expanded fluid gets out of the cylinder as the piston moves back to TDC. Here, suction and discharge processes depend on the valve operations. Hence, valve operations should be precise to achieve timely expansion [11]. Piston expanders are heavy and because of contact movements, create noise and vibrations. Despite these flaws, they have large volumetric ratios and can operate at high pressure and temperature with low speed, and hence are used in small-scale applications [25].

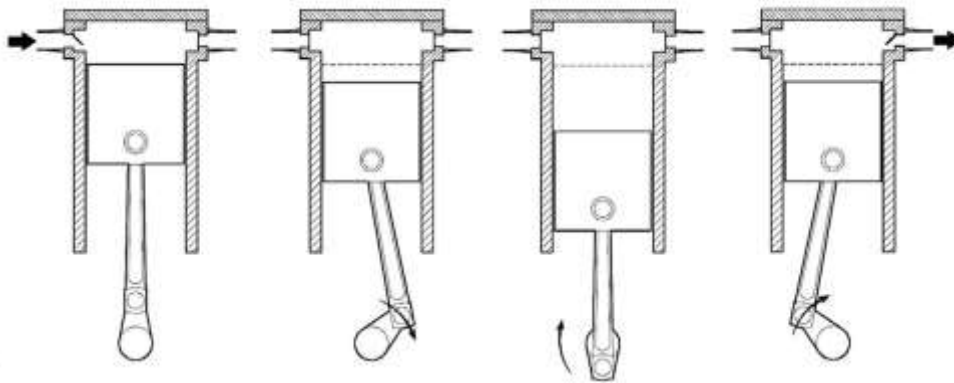


Figure 12: Working of reciprocating piston expander [26]

2.2.5 Free-Piston Expander

Heyl and Quack at Technical University Dresden invented the FPE for the first time in the 1990s [8] [27]. As shown in figure 13, it comprises a dual opposed-piston, connected by a connecting rod and two cylinders. A linear generator (LG) with a series of permanent magnets is mounted on the connecting rod, with coils positioned in the stator. As the intake port on the left opens, working fluid enters the left cylinder and expands, pushing the piston from left to right. After expansion exhaust port on the left opens and simultaneously intake port on the right opens driving in working fluid in the right cylinder and pushing the piston from right to left. During expansion in the right cylinder, expanded fluid from the left cylinder moves out through the exhaust port, completing one cycle. The LG converts mechanical energy into electrical energy. It is more suitable for small-scale applications, among all volumetric types because of good sealing and low frictional losses [8] [27]. There is a lot of research done on the FPE concept, but a lot more is required to put it into practice [8].

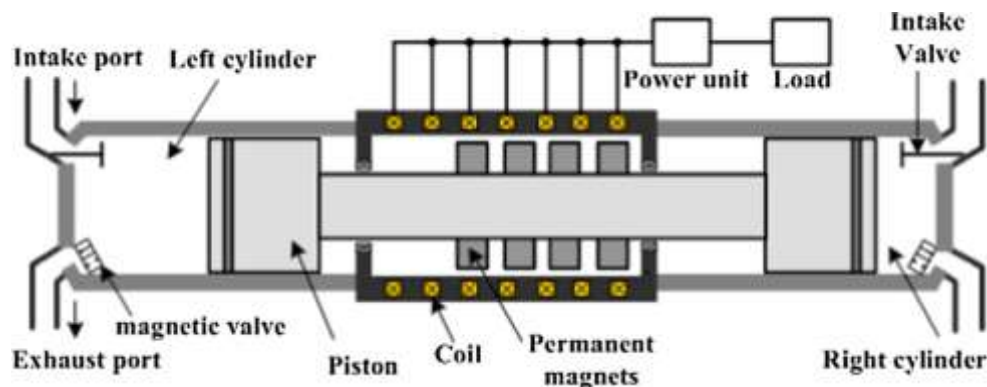


Figure 13: Structure of free-piston linear expander (FPLE) [27]

2.3 Review of Working Fluid Selection Strategies

Research in the field of ORCs' expansion machines and working fluid for WHR is advancing fast. Because of various options available such as hydrocarbons, aromatic hydrocarbons, ethers, perfluorocarbons, Chlorofluorocarbon (CFCs), alcohols, etc, [13], working fluid selection according to the need plays a key role in ORC performance. Screening of suitable working fluids under a given set of conditions is critically studied. As ORC uses different heat sources such as industrial waste heat, solar energy, geothermal energy, waste heat from internal combustion engines (ICEs) [8], and renewables [22] (temperature from 80° C for geothermal to 500° C for biomass), causing the variable working environment, it is complicated to select one suitable working fluid [13].

Working fluids that can be used in an ORC are generally classified as dry (high molecular mass), wet (low molecular mass), and isentropic (medium molecular mass) fluids. The slope of dry, wet, and isentropic working fluid, on the saturation curve ($T-s$), varies due to differences in molecular mass and is sketched in figure 14. If the slope of the saturated vapor curve/ derivative of entropy with respect to temperature is negative, the fluid is called 'wet' fluid, if positive, called 'dry' fluid, and if zero, the fluid is termed as 'isentropic' fluid. If chosen wet fluids, due to the negative slope of the vapor curve, at the expander outlet lots of saturated liquid can be found, which can cause erosion and corrosion of the turbine blades, hence not suitable for turboexpanders if not superheated. Whereas for dry fluids, a superheated expanded vapor is leaving the expander, which increases the condenser load for no reason, and if a regenerator is used to increase efficiency and to lower the condenser load, the initial investment [13] increases significantly. Isentropic fluids show the advantages over dry and wet fluids as they do not require regenerator and superheating due to the vertical slope of the saturation curve [13] and hence are recommended for use. Some examples of dry, wet, and isentropic fluids are given in table 1. Note that the name "isentropic" here does not refer to a process in a cycle, but only to the shape of the saturation curve. While at first confusing, this is a standard nomenclature of the field.

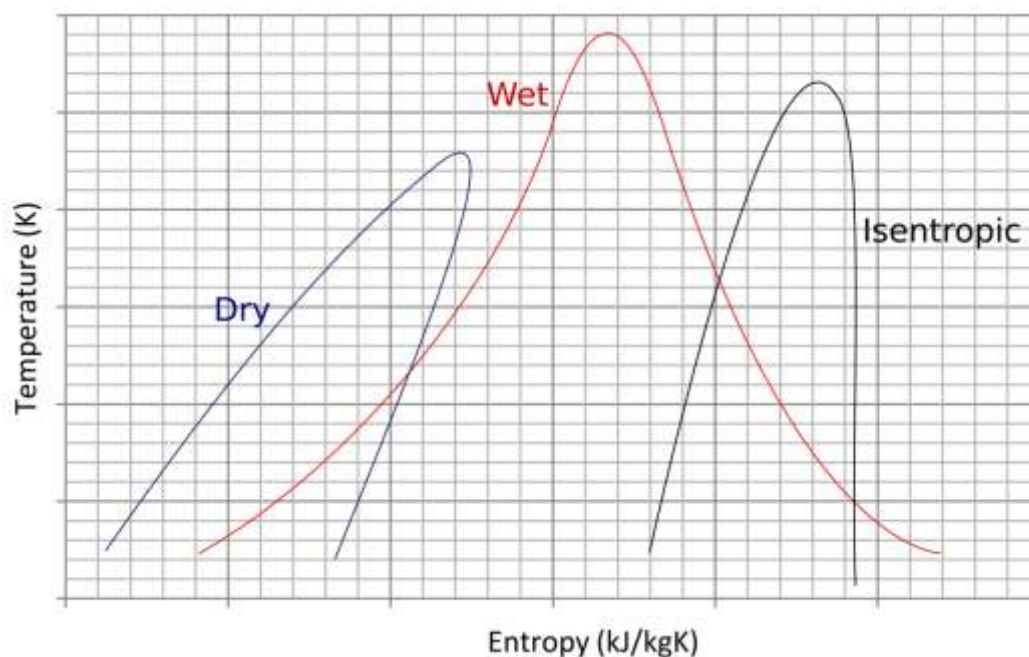


Figure 14: Typical T-s diagram of wet, isentropic, and dry fluids. Classification is based on the slope of the vapor curve [28]

Wet Fluid	Dry Fluid	Isentropic Fluid
Water	Cyclohexane	Trichloromonofluoromethane (R11)
Chlorotrifluoromethane (R13)	Benzene	Dichlorodifluoromethane (R12)
Tetrafluoromethane (R14)	Toluene	Chloropentafluoroethane (R115)
Dichlorofluoromethane (R21)	1,1,2-Trichloro-1,2,2-Trifluoroethane (R113)	Pentafluoroethane (R125)
Chlorodifluoromethane (R22)	1,2-Dichloro-1,1,2,2-Tetrafluoroethane (R114)	1,1,1,2-Tetrafluoroethane (R134a)
Trifluoromethane (R23)	2,2-Dichloro-1,1,1-Trifluoroethane (R123)	1-Chloro-1,1-Difluoroethane (R142b)
Difluoromethane (R32)	1,1-Dichloro-1-Fluoroethane (R141b)	1,1,1-Trifluoroethane (R143a)
Fluoromethane (R41)	1,1,1,2,3,3-Hexafluoropropane (R236ea)	Propane (R290)
Hexafluoroethane (R116)	1,1,1,3,3,3-Hexafluoropropane (R236fa)	
1-Chloro-1,2,2,2-Tetrafluoroethane (R124)	1,1,2,2,3-Pentafluoropropane (R245ca)	
1,1-Difluoroethane (R152a)	1,1,1,3,3-Pentafluoropropane (R245fa)	
Ethane (R170)	Butane (R600)	
Ammonia (R717)	Pentane (R601)	

Table 1: Examples of dry, wet and isentropic fluids

Some of these organic working fluids harm the environment. Fluorinated compounds such as CFCs, Hydrochlorofluorocarbon (HCFCs), and others do not easily react with any other substance available in the environment and dissociate by sunlight/ultraviolet radiation at higher altitudes [29]. Moreover, their lifespan is also long - several years. During the stay in the atmosphere, these compounds trap heat, giving a hand in global warming [30], and when reaching the stratosphere, they react with ozone molecules, causing ozone layer depletion [29]. Due to ozone depletion, ultraviolet (UV-B) rays [31] can enter the earth's atmosphere, boosting the effect of global warming. Moreover, these ultraviolet rays are harmful and can cause skin and eye cancers [31]. During the 1970s, potential risk on the ozone layer due to CFCs was found, and considering the possible risks/harmful effects on the environment and living beings due to ozone layer depletion, in the year 1985, the Vienna Convention was created to perform research activities and share the important outcomes for the protection of human health and environment [32]. In Vienna Convention, there was no mention of any controlling actions for restoration of the ozone layer which is already damaged. Following that the 'Montreal Protocol' was designed to restore the ozone layer by phasing out ozone-

depleting substances (ODS) [33]. The agreement provided more duration to developing countries for the complete phase-out process (production and consumption) than developed countries, details given in table 2. Under the ‘Montreal Protocol’, with few revisions CFCs are phased out and replaced by HCFCs, HCFCs are in process of being phased out and have already been replaced by Hydrofluorocarbon (HFCs) in some applications because of their low ozone depletion potential (ODP; defined below). Despite having low ODP, the Kigali revision to the Montreal protocol adds the HFCs to the list of “banned compounds” because of their high global warming potential (GWP; defined below). It came into effect from the year 2019 to reduce the production and consumption of HFCs over the upcoming years [34]. These HFCs were already on the list of the ‘Kyoto protocol’ for GHGs emission control, which came into force from the year 2005, after the observation of an increase in global mean temperature during the 20th century [35]. Considering the ill effects of such compounds, these treaties came into action for the environmental safety and betterment of all living organisms. Hence, for the fluid selection, various aspects such as ODP, GWP, and atmospheric lifetime (ALT) should be considered [13]. Also, the selected working fluid should be safe to use to avoid any accidents. For safety measures, toxicity and flammability (defined below) of the fluids should be considered. The best-suited fluid is one with zero ODP, small/zero GWP, short ALT, zero toxicity, and lower flammability [36].

ODP: ODP of a substance is the amount of degradation it can cause to the ozone layer relative to the standard compound CFC-11 [30] [37].

GWP: GWP compares the amount of heat trapped by a substance with the amount of heat trapped by the same mass of carbon dioxide [30].

ALT: ALT is the time duration; a substance spends in an atmosphere before getting decomposed [38].

Toxicity: Toxicity is the ability of a substance to cause ill/harmful effects, even with a small amount and short exposure.

Flammability: Flammability is the ability of a substance to self-ignite, creating fire/explosion.

Compounds	Developed countries	Developing countries
	Elimination of production and consumption	
CFCs, Carbon tetrachloride	1996	2010
Halons	1994	2010
Trichloroethane	1996	2015
Methyl bromide	2005	2015
HCFC	2030	2040
Bromochloromethane	2002	2002
	Reduction of production and consumption (% of initial volume)	
HFC	2036 (15%)	2045 (20%) 2047 (15%) *
*Bahrain, India, Iran, Iraq, Kuwait, Oman, Pakistan, Qatar, Saudi Arabia, United Arab Emirates		

Table 2: Phase-out schedule of ODS as per Montreal Protocol [33]

Pure working fluids with zero ODP and small GWP, are highly flammable [15], where the others, which are chemically and operationally stable, have undesirable thermophysical properties [13] [15], show poor cycle performance. Mixtures of different working fluids can be used to enhance the properties of pure fluids for better overall performance. The mixture can be classified as zeotropic and azeotropic based on their behavior. When two compounds, having different boiling point temperatures are mixed and if the mixture reclaims the new boiling point, which can be either high or low from the original boiling point of any compound, they are called ‘azeotropic mixture’ [30] [39]. On the other hand, when both the compounds in a mixture, retain their original boiling point, it is called a ‘zeotropic mixture’ [12] [15] [30] [39]. Azeotropic mixture shows a temperature glide during phase change, thus giving a good thermal match in evaporator and condenser, enhancing overall cycle performance in terms of efficiency and exergy loss [15]. In this regard, pure fluids give constant temperature phase change in an evaporator and condenser, resulting in more exergy losses [15]. This phenomenon is shown in figure 15, for a pure cyclohexane (a) and the mixture of cyclohexane and R123 (b). Due to less research work [12] done on zeotropic mixtures, their use is limited to low-temperature applications [15].

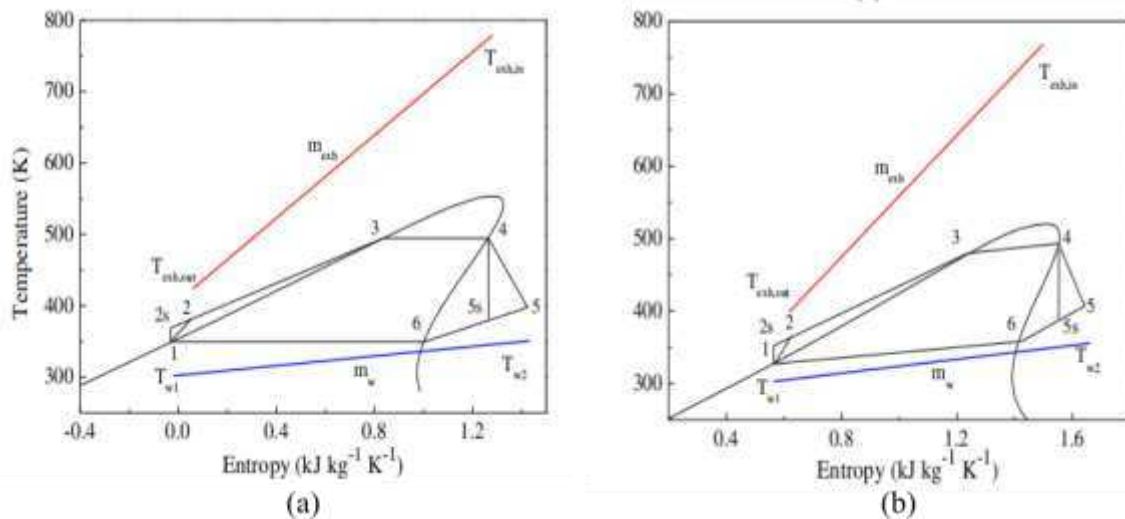


Figure 15: T-s diagram for the ORC for (a) pure cyclohexane and (b) zeotropic mixture of cyclohexane and R123 [15]

To determine the ideal working fluid with the ORC architecture, performance, and expander selection, an optimization process based on thermodynamic [19], chemical [3], and physical [13] properties is also required. Thermodynamic performance, high vapor density, saturation curve, low viscosity, high conductivity, acceptable evaporation pressure, positive condenser gauge pressure, high stability temperature, melting point, ability to dissolve in lubricant oil are a few of many properties that need to be considered while screening candidate fluids for given application [13] [9]. Low vapor density of the working fluid causes higher volume flow rates in the expander, increasing the size of the expander [13]. Fluids with operating pressure lower than atmosphere should be avoided as they stand chances of leakage, affecting performance, and to avoid that, need sealing, which increases overall cost [14]. Fluids with high molecular weight are proven to be advantageous for thermal efficiency [19]. Kuo et al [40] proposed a figure of merit (FOM), which depends on sensible and latent heat of vaporization and predicts the effect on the thermal efficiency that is “smaller the FOM, the larger would be the thermal efficiency”.

$$FOM = Ja^{0.1} \cdot \left(\frac{T_{cond}}{T_{evap}} \right)^{0.8} \quad (2.3.1)$$

where,

$$Ja = \frac{C_p \cdot dT}{Hv}$$

Heat transfer of working fluids with lower heat of vaporization occurs at varying temperatures, shown in figure 16, causing a lower irreversible heat transfer process, thus enhancing overall performance [13].

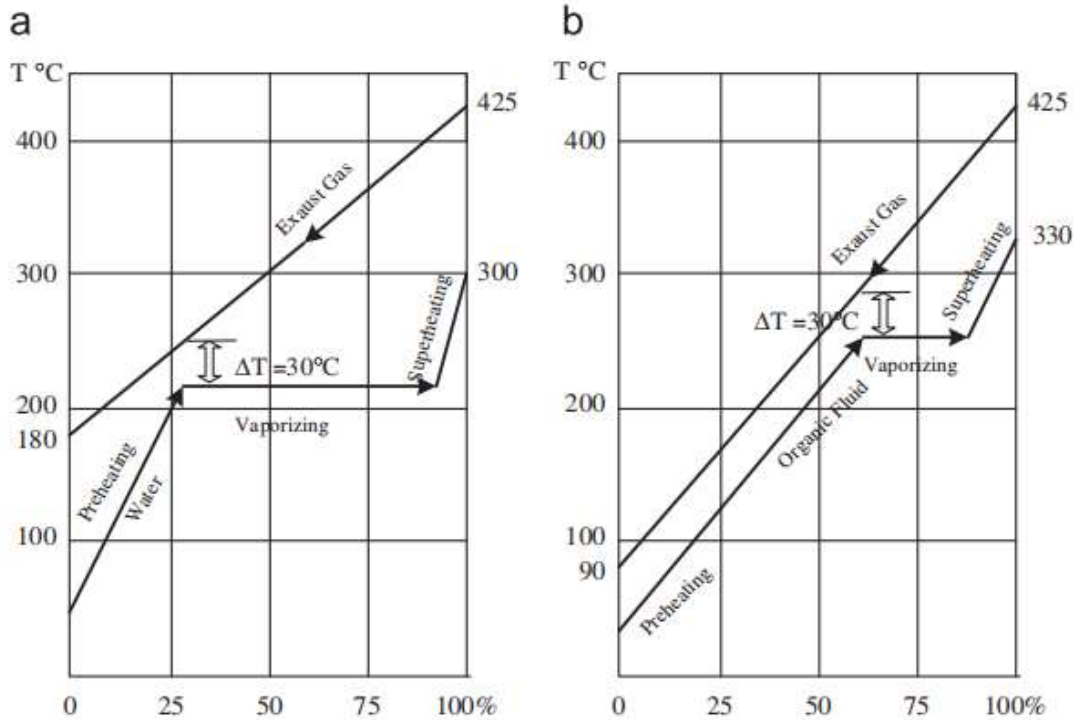


Figure 16: Effect of vaporization heat on the irreversibility in the heat transfer process [13]

Screening of working fluid, with all the above-mentioned considerations, requires an objective function in terms of thermal efficiency, power output, second law efficiency, exergy loss, etc., which can be optimized to get the best overall performance [19] for the specific application. A few optimizations found in the literature are discussed below.

Chao et al [14] came up with a formula to calculate optimal evaporation temperature (OET) of subcritical ORC, to optimize net power output. Twenty-two working fluids were selected and the quadratic approximation method in the engineering equation solver (EES) is used to obtain OETs. Simulated results and calculated results almost matched. The analysis concluded that for larger power output, the critical temperature of the working fluid should approach the waste heat source temperature.

S Douvartzides et al [28] selected 37 working fluids to optimize, for subcritical Rankine cycle for WHR from the exhaust gases of 4 stroke V18 MAN51/60 DF internal combustion engine, driven on natural gas. For optimization, thermodynamic analysis, considering key parameters such as evaporator pressure and superheating temperature is carried out and the conclusion is drawn that for subcritical pressure and non-superheated cycle, increasing evaporation pressure, give higher overall efficiency, but there must be a limit to evaporation pressure

(about 85 - 95% of critical pressure). Hence, fluids with high critical pressure give high efficiency and R32 is selected for the given case.

Wang et al [3] selected nine working fluids to check their performance for recovering engine waste heat with predefined working conditions. To do so, a thermodynamic model was built in MATLAB with REFPROP, and results were compared for selected working fluid when the power output is kept fixed, here 10kW. Analysis was performed for an ideal ORC which uses a single-screw expander, for maintaining high thermal efficiency and fewer exergy losses, to check the influence of various parameters (T_{cond} , T_{evap} , T_{cr} , and n). The analysis concluded that thermal efficiency increases with a decrease in condenser temperature and decreases with a fall in evaporator temperature, though the impact of T_{cond} is much more than T_{evap} , and hence if heat source temperature and condenser temperature is fixed according to the application, efficiency depends on T_{cr} and n , which depends on the molecular composition of a working fluid.

$$\eta_{th} = 1 - \left[\left(\frac{1 - \frac{T_{evap}}{T_{cr}}}{1 - \frac{T_{cond}}{T_{cr}}} \right)^n + \left(\frac{1 - \frac{T_m}{T_{cr}}}{1 - \frac{T_{cond}}{T_{cr}}} \right)^n \cdot \left(\frac{n \cdot \frac{T_m}{T_{cr}}}{1 - \frac{T_m}{T_{cr}}} + 1 \right) \cdot \left(\frac{\frac{T_{evap}}{T_{cr}} - \frac{T_{cond}}{T_{cr}}}{\frac{T_m}{T_{cr}}} \right) \right]^{-1}, \quad (2.3.2)$$

where,

$$T_m = \frac{T_{evap} + T_{cond}}{2},$$

$$n = \left(0.00264 \cdot \frac{L_b}{R \cdot T_b} + 0.8794 \right)^{10} \approx 0.375 - 0.380$$

Shu et al [15] studied the effect of adding mass retardant in hydrocarbons to suppress their flammability, to improve their performance in engine WHR by optimizing thermal efficiency and exergy loss. Results showed that zeotropic mixtures have higher efficiency and lower exergy loss than pure fluids, while azeotropic mixtures show an opposite trend. The analysis concluded that there exists an optimal mixture ratio (OMR) for the different mixtures and that changes with evaporation temperature.

Heberte et al [12] analyzed mixtures of working fluids for geothermal power generation by calculating second law efficiency. Due to the mixture of working fluids, in the evaporator and condenser isothermal phase change occurs, which increases efficiency, decreases the condenser cooling load, and decreases irreversibilities. It is concluded that for the heat source temperature below 120°C, the second law efficiency can be increased by 4.3% to 15%.

There are several parameters/factors, that need attention while selecting a proper working fluid and sometimes trade-offs are required [19] between parameters for better overall performance, with affordable prices and availability at places. Below is the list of the summarized important considerations.

- Impact on the environment
- Thermodynamic, physical, and chemical properties
- Availability and handling
- Economic feasibility
- Cycle performance

Keeping in mind all the above-mentioned factors, choosing a suitable working fluid is a very complex task. The opposite approach can be used to make the procedure a little bit simple. In that case, for the given application (cycle, expander type, hot source temperature, condensation temperature), the objective function can be selected and optimized, obtain a list of suitable fluids, and then considering fluid properties, availability, and impact on the environment, fluids can be deduced from the list to get the best-suited one.

2.4 Review of Free Piston Expander Cycles

For recovering waste heat, it is hard to build the most efficient ORC without an appropriate expander [8]. For small-scale WHR, turboexpanders are not suitable because of their high speed [26] (lowers the power output [41]) and large enthalpy drop across the expander [22], but volumetric expanders such as scroll, screw, vane, reciprocating piston, etc. can be used [11] [41]. Each expander has its advantages and disadvantages and is suitable according to the working conditions and type of application. To select the best-suited expander device, several factors, such as power output, isentropic efficiency, expansion ratio, lubrication requirements, complexity, dynamic balance, reliability, cost, working temperature and pressure, leakage, noise, safety [41] should be considered. After the development of FPE in the 1990s, for the enhancement of ORC technology, research to implement FPE in it for WHR and performance comparison with other expanders has been started. After a literature search on expander technologies, Tian et al [41], Li et al [42], and Hou et al [43] stated that FPE is the most promising technology due to its advantages of low friction, simple structure, and a good sealing with the added advantages of a reciprocating piston expander (large built-in volume ratio, high operating pressure and temperature and low speed [25]). Few existing FPE implementations and research findings are discussed below.

2.4.1 Existing FPE Implementations

Wang et al [27] developed an air-driven free piston expander linear generator (FPE-LG) to analyze its performance and potential advantages, and to provide a base for future development of FPE-LG for specific applications. Li et al [42] developed FPE-LG for WHR from internal combustion engine exhaust, performed experiments on the air test rig, and after comparing experimental results with simulation results, concluded that FPE-LG is feasible to use for WHR. Tian et al [41] developed single-piston FPE-LG for ORC, for recovering heat and improving the efficiency of ICEs. Investigation revealed that it has continuous and stable operation and hence is feasible to use. Burugupally et al [44] developed and investigated the performance of miniature FPE working with an open cycle and concluded that miniature FPE is favorable for low-temperature WHR.

2.4.2 Efficiency and Performance Predictions and Calculations

Champagne et al [45] studied the previous work done on small-scale free-piston engines and problems associated with them, where internal combustion was the driving force. They proposed an alternative approach where the engine is driven by external combustion and optimized variables such as piston length-mass, FPE shape-size, input pressure, and lubrication. The analysis concluded that piston shape does not affect the natural frequency of operation, Circular pistons have reliable motion, lubrication should be viscous enough to seal, but not that viscous which in turn hinders the piston motion.

Preetham et al [46] derived a nonlinear lumped parameter model to study the controlling factors of the FPE engine cycle using properties of the fluid 3MTM, HFE-7200 (NOVEC Engineered Fluid). By varying operating parameters such as heat input, external load, and piston mass,

trends for optimal performance were obtained. The results concluded that by increasing input heat rate and injection pressure, work output increases, with simultaneous decreases in operating frequency. The increasing load did not affect work output and efficiency but lowered the operating frequency. The effect of varying piston mass on efficiency, power output, and operating frequency is shown in Figures 17 and 18. To achieve high thermal efficiency, it is suggested to use a higher piston mass.

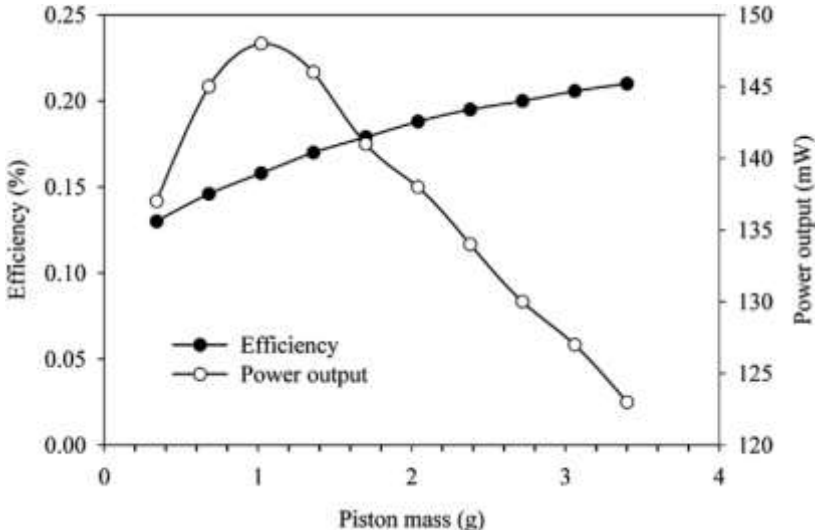


Figure 17: Efficiency and output power dependency on piston mass [46]. Note the efficiency is wrongly reported to be a percentage and is instead in decimal form.

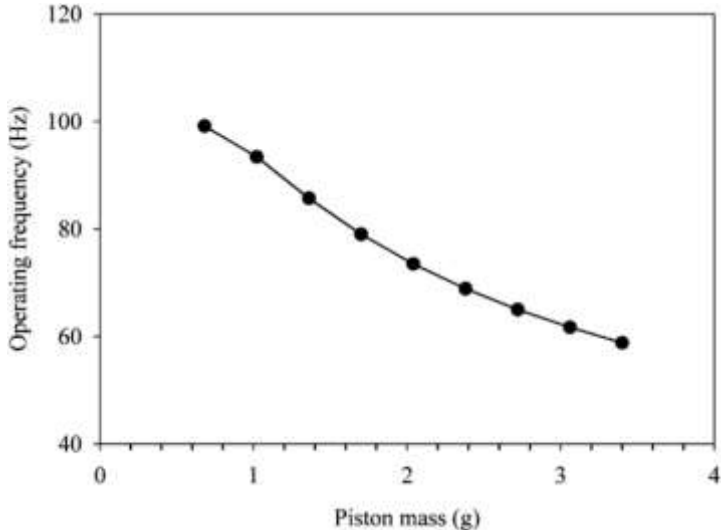


Figure 18: Operating frequency dependency on piston mass for fixed input heat $E = 10\text{mJ/cycle}$ and load $b = 1\text{Ns/m}$ [46]

Hou et al [43] developed and investigated the FPE-LG for ORC and performed experiments on the air test rig. From the results, parameters affecting the performance of FPE-LG are listed, such as intake pressure, external load, and operating frequency.

3 Matched Steady-Unsteady Thermodynamic Cycle Analysis

Thermodynamic devices, especially for power generation from traditional sources or for heat recovery, are traditionally, purely, steady devices, e.g. turbo-expanders. The rising interest for piston-based heat recovery systems requires the matching of a steady heat recovery (also known as a heat exchanger) system with an unsteady expander. This is especially true for the FPE, where the expansion ratio may vary in the course of the operation and the intrinsic unsteadiness of the device may be exploited to accommodate varying loads and conditions.

Searching through the literature, no method or analysis was found that matches unsteady and steady processes for the expander of an ORC. This analysis incorporates the steady and unsteady processes for an ideal, mass-less, double-acting FPE.

3.1 Overview of Cycle Processes

An FPE is a positive displacement device and requires a certain time to be filled, expand and produce work. As mass flow is not continuous in an FPE based ORC, during the expansion of the working fluid, new mass is not coming in and hence the boiler/heat exchanger starts to get pressurized. Conversely, the condenser pressure lowers momentarily. To avoid the problem of pressurizing/depressurizing, two large tanks must be used after the boiler and before the condenser. These act as a capacitor to feed the condenser and to maintain the pressure in the boiler, while the piston is closed. Another option is to use several FPEs such that one piston is always accepting and rejecting fluid.

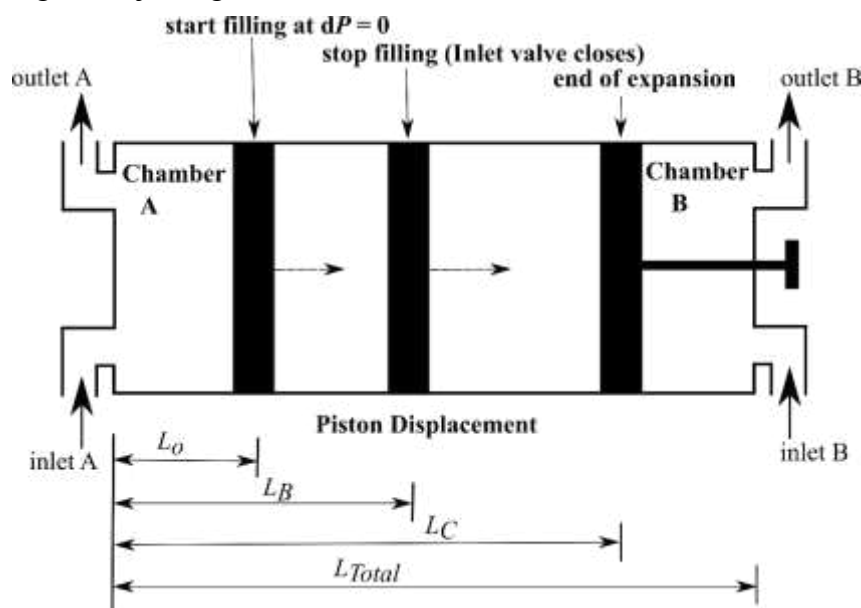


Figure 19: Piston displacement [double acting FPE]

In one FPE cycle, the piston starts a distance L_0 from the end wall, at which point the inlet valve opens and fluid fills the system rapidly at constant volume. The piston then travels to a distance L_B while undergoing constant pressure filling. The inlet valve is closed at position L_B and the high-pressure system expands until the piston reaches L_C . Throughout this movement, the opposing chamber B is at the constant condenser pressure and its exhaust valve is opened. At position L_C , the exhaust valve of chamber A is opened. The exhaust valve of chamber B closes and the intake valve opens. The chamber roles are reversed and the piston travels back to L_0 , thus completing one cycle.

Two important parameters will control the efficiency and power output: the fill ratio, $r_f = L_o/L_B$, and the expansion ratio, $r_p = L_C/L_B$.

Certain assumptions are made: the piston is mass-less, hence the kinetic and potential energy of the device is negligible; the kinetic and potential energy of the working fluid is negligible; the working fluid is expanded isentropically in the FPE; all processes in the expander (filling at constant volume and constant pressure, expansion, etc.) are adiabatic; and the expander has perfect seals, hence no leakage takes place. All thermodynamic equations of state (EOS) are obtained, here, from the COOLPROP reference database. This tool is a combination of EOS models and reference data that can calculate thermodynamic states for, at this moment, 123 different pure fluids. This validated, open-source tool is a convenient alternative to the NIST REFPROP database.

For this analysis, it is considered that saturated working fluid at temperature T_1 and pressure $P_C = P_1$ is pumped to the heat exchanger pressure $P_B = P_2$ (1→2). There, it is heated up using energy from the waste heat to the temperature T_{3p} at a constant boiler pressure (2→3p). The WF then enters cylinder A of the double-acting FPE, initially at constant volume, $dV = 0$ (dashed lines, 3p→3a). The WF undergoes a temperature jump from T_{3p} to T_{3a} . After this constant volume filling process, the WF keeps entering cylinder A at constant pressure, $dP = 0$. The WF temperature thereby drops to T_{3b} . After the entire filling process, the inlet valve is closed and the working fluid expands isentropically until it reaches the pressure $P_{expanded}$. At the same time, cylinder B of FPE is rejecting WF at the constant condenser pressure. After expansion in cylinder A, working fluid is pushed out of the FPE at constant condenser pressure P_4 . Simultaneously, cylinder B of the FPE starts filling, first at constant volume and then at constant pressure. The exhaust valve of chamber A is opened, the chamber vents to the condenser pressure P_4 , and the WF that was expelled from the FPE losses heat in the condenser, is routed to the pump, and the cycle repeats.

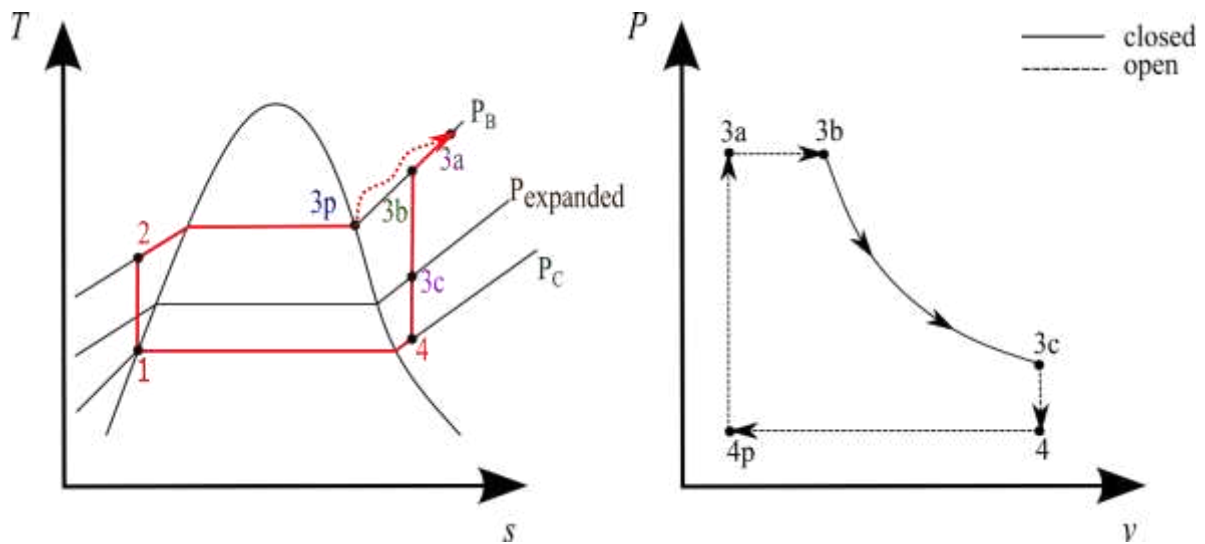


Figure 20: $T-s$ and $P-v$ diagram

3.2 Steady Processes

For the steady processes, 1 to 2, 2 to 3, and 4 to 1, the classical analysis is used. For condensation from 4 to 1, the heat rejected is

$$\dot{Q}_{out} = \dot{m} \cdot (h_4 - h_1), \quad (3.2.2)$$

where state 1 is the saturated liquid state at P_C . For compression from 1 to 2, the required work is

$$\dot{W}_{in} = \dot{m} \cdot (h_2 - h_1), \quad (3.2.3)$$

Finally, the evaporation occurs at constant pressure and the required heat input is

$$\dot{Q}_{in} = \dot{m} \cdot (h_{3p} - h_2), \quad (3.2.4)$$

where h_{3p} can be selected. In the current work, state 3p is fixed on the saturated vapor line. Although the model can account for a mixture or for superheating as the output of the boiler.

3.3 Unsteady Processes

The unsteady processes that need to be analyzed are, $3p \rightarrow 3a$, $3a \rightarrow 3b$, $3b \rightarrow 3c$ and $3c \rightarrow 4$. For the constant volume, $dV = 0$, injection process of WF from $3p \rightarrow 3a$, the final pressure is equal to the boiler pressure,

$$P_{3p} = P_{3a}. \quad (3.3.1)$$

For the constant pressure, $dP = 0$, injection process of WF from $3a \rightarrow 3b$, work output due to change in control volume from V_{3a} to V_{3b} is

$$W_{out,dP=0} = P_B(V_{3b} - V_{3a}). \quad (3.3.2)$$

For both injection processes, the incoming fluid is at the boiler state, 3p. For the isentropic expansion from $3b \rightarrow 3c$, work output is

$$W_{out,expansion} = U_{3b} - U_{3c}. \quad (3.3.3)$$

During the isentropic expulsion of the WF from the cylinder, from $3c \rightarrow 4$, the work required is

$$W_{expulsion} = P_C(V_{3c} - V_4), \quad (3.3.5)$$

where $V_4 = V_{3a}$, because of the double-acting nature of the FPE.

The states 3a, 3b, 3c and 4 cannot be determined independently. One must solve for the states simultaneously.

3.3.1 State Determination

Working fluid is injected at a constant volume ($3p \rightarrow 3a$) and constant pressure ($3a \rightarrow 3b$) in the FPE. Some residue of fluid is seen in the cylinder from the previous cycle, which has the same properties as that fluid at state 4 (condenser entrance). The filling of FPE is an open system and with the above-stated assumptions, thermodynamic analysis can be carried out for both processes.

3p - 3a: Filling of the FPE; Adiabatic Mass Injection at $dV=0$

During the filling of FPE at constant volume (shown in figure 21), the residue and fresh working fluid mix. The end state of the working fluid is state 3a, where we can potentially get a temperature jump. The fluid entering the FPE possesses the properties of state 3p (heat exchanger outlet) and the residue has the properties of state 4. The first law of thermodynamics for the open system can be written as below.

$$\frac{dE}{dt} = \dot{Q} - \dot{W} + \dot{m} \cdot h_{in}$$

During the constant volume filling process, there is no heat (adiabatic) and work transfer.

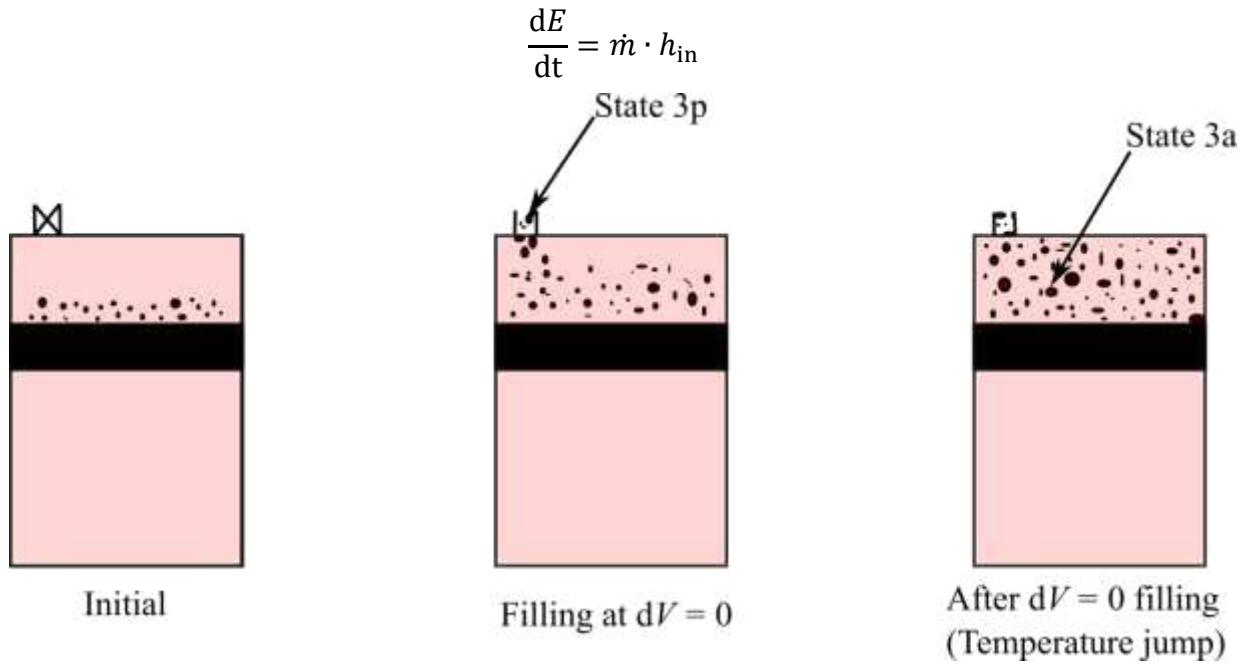


Figure 21: Adiabatic filling process of working fluid at constant volume

The integration

$$\int_i^f \frac{dE}{dt} = h_{in} \cdot \int_i^f \dot{m}$$

yields

$$m_f \cdot u_f - m_i \cdot u_i = h_{in} \cdot \Delta m.$$

Dividing by initial volume yields

$$\rho_f \cdot u_f - \rho_i \cdot u_i = h_{in} \cdot \Delta \rho.$$

Rearranging and recognizing that $h_{in} = h_{3p}$, $u_i = u_4$, $\rho_i = \rho_4$, $u_f = u_{3a}$ and $\rho_f = \rho_{3a}$,

$$h_{in} = h_{3p} = \frac{\rho_{3a} \cdot u_{3a} - \rho_4 \cdot u_4}{\rho_{3a} - \rho_4}. \quad (3.3.1.1)$$

The same equation can be expressed for u_{3a} such that the full state is

$$u_{3a} = \frac{(\rho_{3a} - \rho_4) \cdot h_{3p} + \rho_4 \cdot u_4}{\rho_{3a}}, P_{3a} = P_{3p} \quad (3.3.1.2)$$

3a - 3b: Filling of the FPE; Adiabatic Mass Injection at $dP=0$

During the filling of the FPE at constant pressure (shown in figure 22), the WF in the chamber at state 3a and the incoming fresh working fluid are mixed. The inlet valve closes when the piston reaches point B. The fluid entering the FPE is the same as before and possesses the properties of state 3p (heat exchanger outlet), while the WF mixture in FPE has properties of state 3a. The first law of thermodynamics for the open system is

$$\frac{dE}{dt} = \dot{Q} - \dot{W} + \dot{m} \cdot h_{in}.$$

During the constant pressure filling process, there is no heat (adiabatic) transfer but work is being done.

$$\frac{dE}{dt} = -\dot{W} + \dot{m} \cdot h_{in}.$$

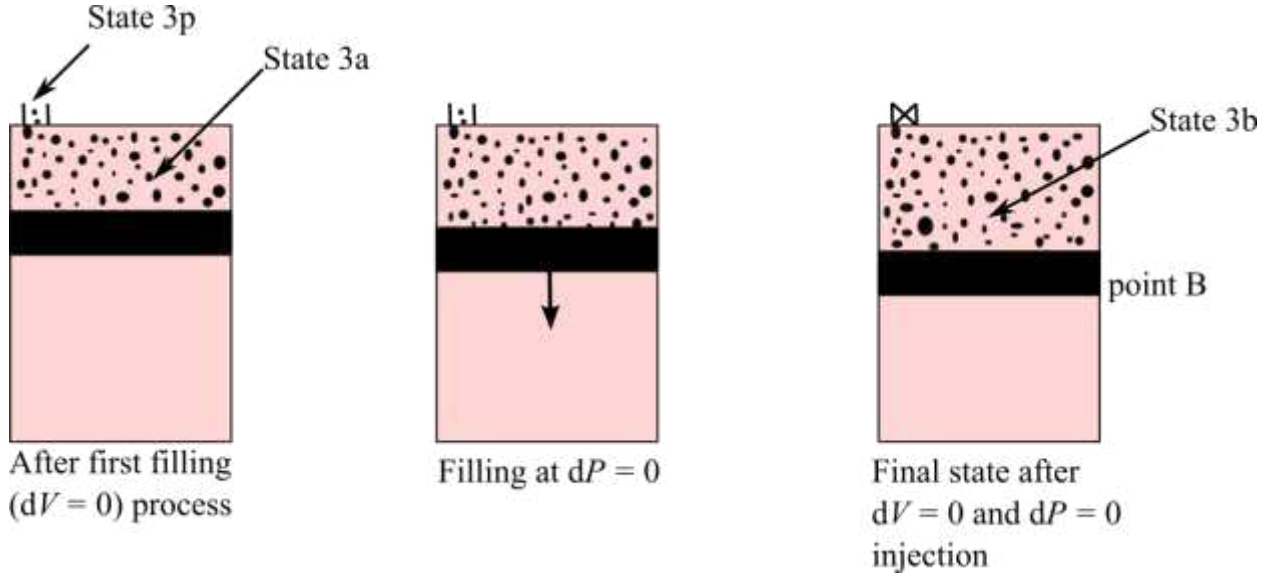


Figure 22: Adiabatic filling process of working fluid at constant pressure

The integration

$$\int_i^f \frac{dE}{dt} = - \int_i^f \dot{W} + h_{in} \cdot \int_i^f \dot{m}$$

yields

$$m_f \cdot u_f - m_i \cdot u_i = -P_B(v_f \cdot m_f - v_i \cdot m_i) + h_{in} \cdot \Delta m,$$

since the work is at constant pressure. As $u + Pv = h$ and recognizing that $h_{in} = h_{3p}$, $h_i = h_{3a}$, $m_i = m_{3a}$, $h_f = h_{3b}$ and $m_f = m_{3b}$

$$m_{3b} \cdot h_{3b} - m_{3a} \cdot h_{3a} = h_{3p} \cdot (m_{3b} - m_{3a}). \quad (3.3.1.3)$$

The mass, $m = V\rho$ and volumes can be expressed from the piston displacement diagram (figure 19), $V_{3b} = L_B \cdot A_p$ and $V_{3a} = L_o \cdot A_p$.

Inserting the above in equation (3.3.1.3), yields

$$u_{3a} = \frac{\frac{1}{r_f} [\rho_{3b} \cdot h_{3b} - h_{3p} \cdot (\rho_{3b} - r_f \cdot \rho_{3a})] - P_B}{\rho_{3a}}, P_{3b} = P_{3p} \quad (3.3.1.4)$$

where $r_f = L_o / L_B$.

Comparing Eq. (3.3.1.2) and (3.3.1.4), the following is obtained:

$$P_B = \frac{\rho_{3b}}{r_f} (h_{3b} - h_{3p}) - \rho_4 (u_4 - h_{3p}). \quad (3.3.1.5)$$

As mentioned earlier, the EOS used for calculating all the state points is from the COOLPROP database. The EOS derived for all fluids are based on Helmholtz energy formulations. These EOS are valid for the whole fluid range, from subcooled liquid to supercritical vapor. All state points can be calculated for known T_{hot} , T_{cold} , r_f , and r_p , by the following two iterative procedures. First,

1. Pick the value of s_4 and determine the state 4 and state 3b from (P_C, s_4) and (P_B, s_4) respectively.

2. Calculate P_B using equation (3.3.1.5).
3. Compare the value of the calculated P_B with the actual P_B .
4. Repeat the procedure until the value of P_B matches.
5. From the optimized s_4 , states 3b, 3c and 4 can be known.

For calculating state 3a, the second iterative procedure is as follows.

1. Pick the value of u_{3a} and determine the state 3a from (P_B, u_{3a}) .
2. Calculate ρ_{3a} using equation (3.3.1.2) or (3.3.1.4).
3. Compare the value of calculated ρ_{3a} with the one determined with assumed u_{3a} .
4. Repeat the procedure until the value of ρ_{3a} matches.
5. From the optimized u_{3a} , state 3a can be known.

3.4 Specific Work Output and Efficiency

The net expander work output to the shaft is the summation of the work out due to constant pressure filling, work out due to expansion and work required for expulsion of WF.

$$W_{\text{out}} = W_{\text{out,dP=0}} + W_{\text{out,expansion}} - W_{\text{expulsion}} \quad (3.4.1)$$

or

$$W_{\text{out}} = P_B(V_{3b} - V_{3a}) + U_{3b} - U_{3c} - P_C(V_{3c} - V_{3a}). \quad (3.4.2)$$

$$W_{\text{out}} = P_B(m_{3b} \cdot v_{3b} - m_{3a} \cdot v_{3a}) + m_{3b} \cdot u_{3b} - m_{3c} \cdot u_{3c} - P_C(m_{3c} \cdot v_{3c} - m_{3a} \cdot v_{3a}).$$

The amount of injected mass, m_{inj} , considers the residual mass m_4 from the previous cycles, $m_{\text{inj}} = m_{3b} - m_4$

The work done by the expander, per mass injected is then

$$\dot{W}_{\text{out}} = \frac{W_{\text{out}}}{m_{\text{inj}}} \quad (3.4.3)$$

or

$$\dot{W}_{\text{out}} = P_B \left(\frac{m_{3b}}{m_{\text{inj}}} \cdot v_{3b} - \frac{m_{3a}}{m_{\text{inj}}} \cdot v_{3a} \right) + \frac{m_{3b}}{m_{\text{inj}}} \cdot u_{3b} - \frac{m_{3c}}{m_{\text{inj}}} \cdot u_{3c} - P_C \left(\frac{m_{3b}}{m_{\text{inj}}} \cdot v_{3c} - \frac{m_{3a}}{m_{\text{inj}}} \cdot v_{3a} \right).$$

All mass ratios are needed to complete the model. The mass injected during the constant volume filling process is

$$m_{\text{dv}} = m_{3a} - m_4 = \rho_{3a} \cdot V_0 - \rho_4 \cdot V_0 = (\rho_{3a} - \rho_4) \cdot r_f \cdot L_B \cdot A_P.$$

The mass injected during the constant pressure filling process is

$$m_{\text{dp}} = m_{3b} - m_{3a} = \rho_{3b} \cdot L_B \cdot A_P - \rho_4 \cdot L_0 \cdot A_P = (\rho_{3b} - \rho_{3a} \cdot r_f) \cdot L_B \cdot A_P.$$

The total mass injected in a cycle is then

$$m_{\text{inj}} = m_{\text{dv}} + m_{\text{dp}} = L_B \cdot A_P \cdot [(\rho_{3a} - \rho_4) \cdot r_f + (\rho_{3b} - \rho_{3a} \cdot r_f)] = L_B \cdot A_P \cdot (\rho_{3b} - \rho_4 \cdot r_f).$$

The residual mass in the FPE at the start of the cycle is

$$m_4 = L_0 \cdot A_P \cdot \rho_4.$$

The mass in the FPE, after the constant volume injection process is

$$m_{3a} = L_O \cdot A_P \cdot \rho_{3a}.$$

The mass ratios needed to calculate the work output from the expander are thus;

$$\frac{m_{3a}}{m_{inj}} = \frac{L_O \cdot A_P \cdot \rho_{3a}}{L_B \cdot A_P \cdot (\rho_{3b} - \rho_4 \cdot r_f)} = \frac{r_f \cdot \rho_{3a}}{\rho_{3b} - \rho_4 \cdot r_f}, \quad (3.4.4)$$

$$\frac{m_4}{m_{inj}} = \frac{L_O \cdot A_P \cdot \rho_4}{L_B \cdot A_P \cdot (\rho_{3b} - \rho_4 \cdot r_f)} = \frac{r_f \cdot \rho_4}{\rho_{3b} - \rho_4 \cdot r_f}, \quad (3.4.5)$$

$$\frac{m_{3b}}{m_{inj}} = \frac{m_4 + m_{inj}}{m_{inj}} = \frac{r_f \cdot \rho_4}{\rho_{3b} - \rho_4 \cdot r_f} + 1 = \frac{\rho_{3b}}{\rho_{3b} - \rho_4 \cdot r_f}. \quad (3.4.6)$$

The efficiency can then be calculated using the following equation,

$$\eta = \frac{\dot{W}_{out} - \dot{W}_{in}}{\dot{Q}_{in}} = \frac{\dot{W}_{out} - (h_2 - h_1)}{(h_{3p} - h_2)}. \quad (3.4.7)$$

3.5 Length and Time Scale Calculations

Every quantity determined so far is specific and independent of the extent of the system. A specific, physical FPE has scales of power, P_{target} , length through the area of the piston, A_P , or its diameter, D_p , and velocity, $v_{P,max}$. The maximum velocity scale is imposed by the electrical generator mounted to the FPE. Currently, the limit is on the order of 2-5 m/s.

3.5.1 Targeted Power and Piston Diameter

The power output at any instant is given by,

$$P_{target} = (P(t) - P_C) \cdot v_P(t) \cdot A_P, \quad (3.5.1.1)$$

and a requirement of the application is that it should be constant. The FPE is constrained by maximum velocity $v_{P,max}$, which occurs at P_{3c} , the pressure at the end of the expansion. Hence, for constant targeted power output,

$$P_{target} = (P_{3c} - P_C) \cdot v_{P,max} \cdot A_P \quad (3.5.1.2)$$

Equation (3.5.1.2) yields the piston area and subsequently piston diameter.

3.5.2 Cycle Time

The FPE is also constrained by the maximum operating frequency f , and hence cycle time τ . Calculating the total cycle time $\tau/2 = \tau_{fill} + \tau_{exp}$ fixes the physical extent of the FPE. For a constant power output, the pressure and velocity are related,

$$(P_{3c} - P_C) \cdot v_{P,max} \cdot A_P = (P_B - P_C) \cdot v_{P,fill} \cdot A_P.$$

The velocity during the fill is then

$$v_{P,fill} = \frac{(P_{3c} - P_C)}{(P_B - P_C)} \cdot v_{P,max}.$$

Hence,

$$\tau_{fill} = \frac{(L_B - L_O)}{v_{P,fill}} = \frac{L_B(1 - r_f) \cdot (P_B - P_C)}{(P_{3c} - P_C) \cdot v_{P,max}} \quad (3.5.2.1)$$

The velocity of the piston at any instant of expansion is

$$v_P(t) = \frac{(P_{3c} - P_C)}{(P(t) - P_C)} \cdot v_{P,\max} = \frac{dx}{dt}$$

Integrating for expansion (3b-3c) yields

$$\int_0^{\tau_{\text{exp}}} dt = \int_{L_B}^{L_C} \frac{(P(t) - P_C)}{(P_{3c} - P_C) \cdot v_{P,\max}} dx = \tau_{\text{exp}}$$

Defining $\varepsilon = \frac{x}{L_B}$ and $d\varepsilon = \frac{1}{L_B} dx$; New limits of integration are used: at $x = L_B$, $\varepsilon = 1$, and at $x = L_C$, $\varepsilon = r_p$.

The integration is then,

$$\tau_{\text{exp}} = \frac{L_B}{(P_{3c} - P_C) \cdot v_{P,\max}} \int_1^{r_p} (P(\varepsilon) - P_C) d\varepsilon \quad (3.5.2.2)$$

Hence, the total time for one cycle is

$$\frac{\tau}{2} = \tau_{\text{fill}} + \tau_{\text{exp}}. \quad (3.5.2.3)$$

Inserting values from equations (3.5.2.1) and (3.5.2.2),

$$\frac{\tau}{2} = \frac{(P_B - P_C) \cdot L_B}{(P_{3c} - P_C) \cdot v_{P,\max}} [(1 - r_f) + \int_1^{r_p} \frac{(P(\varepsilon) - P_C)}{(P_B - P_C)} d\varepsilon] \quad (3.5.2.4)$$

From Equation (3.5.2.4), L_B can be calculated and the total length of the FPE can be determined using the equation given below,

$$L_{\text{Total}} = L_C + L_O = \left(\frac{L_C}{L_B} + \frac{L_O}{L_B} \right) \cdot L_B = (r_p + r_f) \cdot L_B. \quad (3.5.2.5)$$

4 Result and Analysis

The behavior of the model and device over a range of design/operating parameters and use cases is first examined. To achieve this, changes in the state of the system, efficiency, the power output are analyzed. Four fluids (R1234yf, Novec649, Toluene, Water) are selected as representative of the range of potentially useful fluids for the constraints $T_{\text{hot}} = 348 \text{ K}$ and $T_{\text{cold}} = 293 \text{ K}$. The influence of the cycle parameters r_f , r_p , T_{hot} and T_{cold} on efficiency and physical design is examined.

4.1 Impact of Expansion Ratio, r_p

First, keeping fill ratio constant, $r_f = 0.1$, the effect of expansion ratio, r_p , on cycle efficiency is studied. This fixed value of r_f is not significant and is selected based on the intuition of the expected behavior of a realizable machine. As seen in figure 23, for a given r_f , the thermal efficiency increases and reaches a maximum for each fluid. This maximum efficiency occurs at the maximum expansion ratio, $r_{p,\text{max}}$, that can be attained. This maximum expansion ratio corresponds to the expansion ratio at which the final pressure in the cylinder is equal to the condenser pressure. Further movement, beyond $r_{p,\text{max}}$, would result in overexpansion, a decrease of the cylinder pressure below the condenser pressure, and a decrease in efficiency. For R1234yf, the maximum efficiency is 0.12163 at an expansion ratio of 4.6816. For toluene and water 0.13951 and 0.14735 at r_p of 9.4809 and 12.2116 respectively. On the other hand, for novect649, the maximum attainable efficiency is only 0.11199 at an expansion ratio of 7.3396.

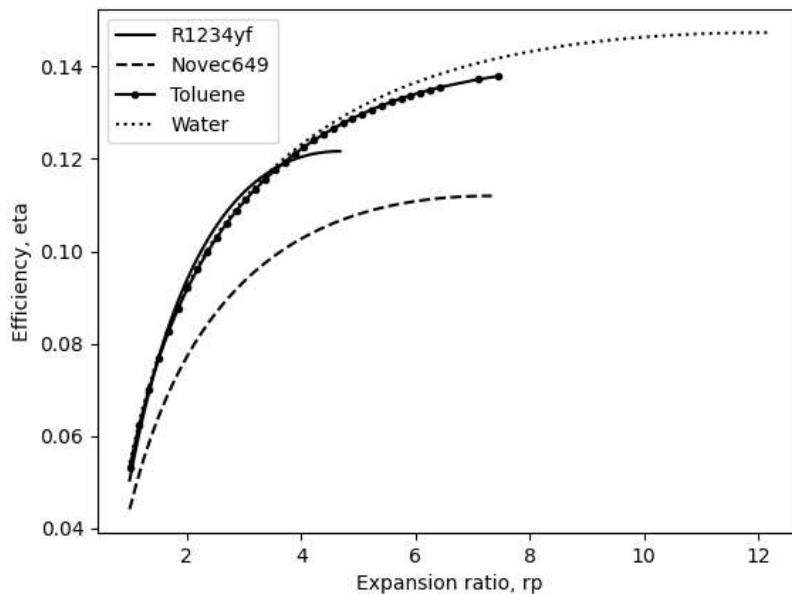


Figure 23: Variation in efficiency with expansion ratio for a given $r_f = 0.1$. The incomplete line for toluene is due to the failure of Brent's method.

4.2 Impact of Fill Ratio, r_f

The effect of fill ratio, r_f is studied independently for a fixed $r_p = 2$. Figure 24 shows that thermal efficiency decreases monotonically with increasing fill ratio, r_f for all fluids. The efficiency decreases by 49.8% for R1234yf, 53.7% for toluene, 50.1% for water, and 53.5% for novect649.

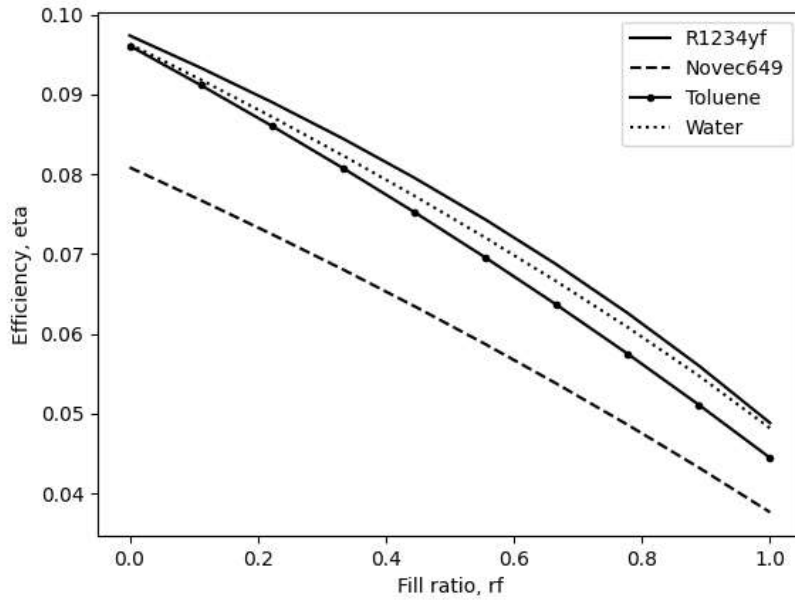


Figure 24: Variation in efficiency with fill ratio for a given $r_p = 2$

To understand the negative effect of fill ratio on efficiency, the variations in temperature at different points of the cycle (3p, 3a, 3b and 3c) with varying fill ratio is examined and shown in figure 25, 26, 27 and 28 for R1234yf, novec649, toluene and water respectively. Point 3p is kept fixed on the saturated vapor line and hence that temperature remains constant despite the change in fill ratio. Point 3a is achieved after the constant volume filling, during which a temperature jump is achieved. This temperature T_{3a} , with increasing fill ratio increases. After constant volume filling, fluid is injected at constant pressure (until point B), during which the temperature drops in the cylinder due to the mixing of WFs. With the increase in fill ratio, temperature T_{3b} increases. At a fill ratio of 1, $T_{3a} = T_{3b}$. The temperature T_{3c} , is the temperature after expansion. For a fixed expansion ratio, r_p of 2, T_{3c} is increasing (can be seen in figure 25, 26, 27 and 28) and pressure after the expansion is moving towards condenser pressure. At a fill ratio of 1, though the temperature jump achieved is higher, the pressure after expansion also goes down towards the condenser pressure, instead of increasing efficiency, it gives a negative effect on efficiency. The reason behind that is the increase in area under $T - s$ curve, for work output the increase in area is smaller than the increase for condenser work shown in figure 29.

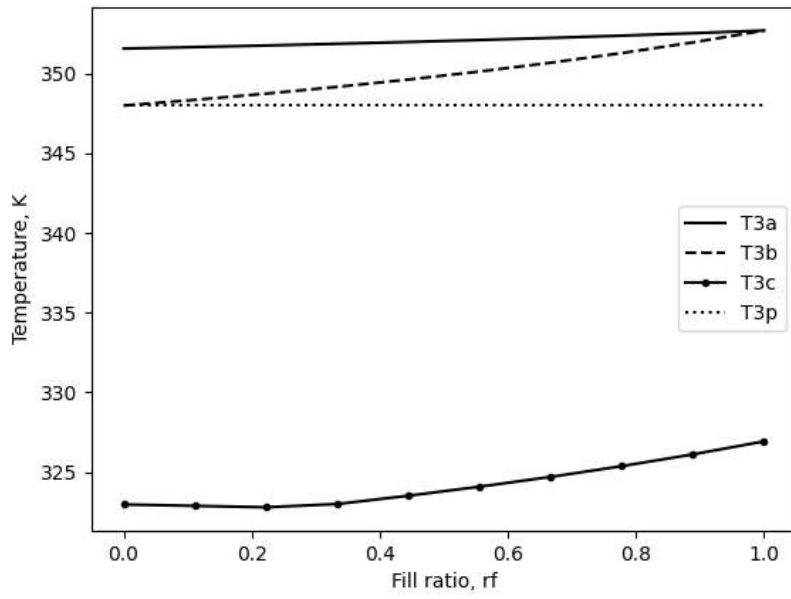


Figure 25: Variation in temperatures (at points p, a, b and c) with fill ratio, at $r_p = 2$ for R1234yf

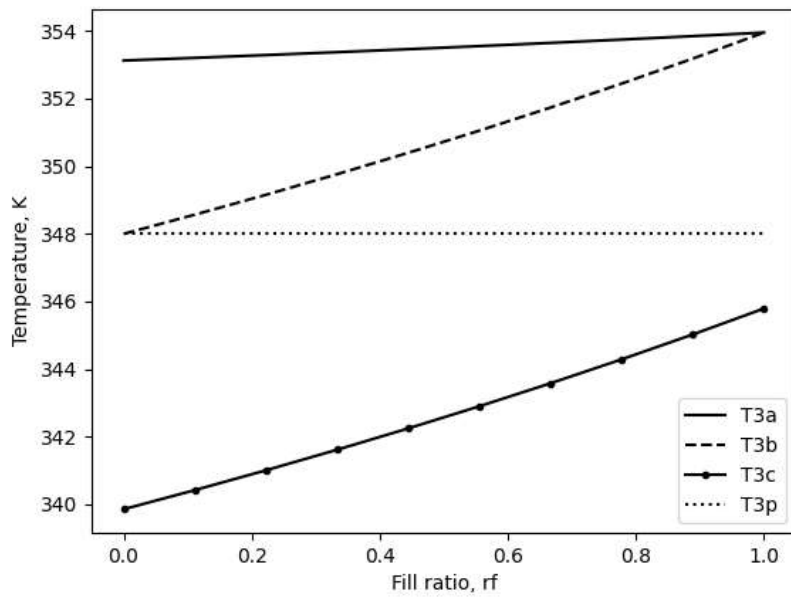


Figure 26: Variation in temperatures (at points p, a, b and c) with fill ratio, at $r_p = 2$ for novvec649

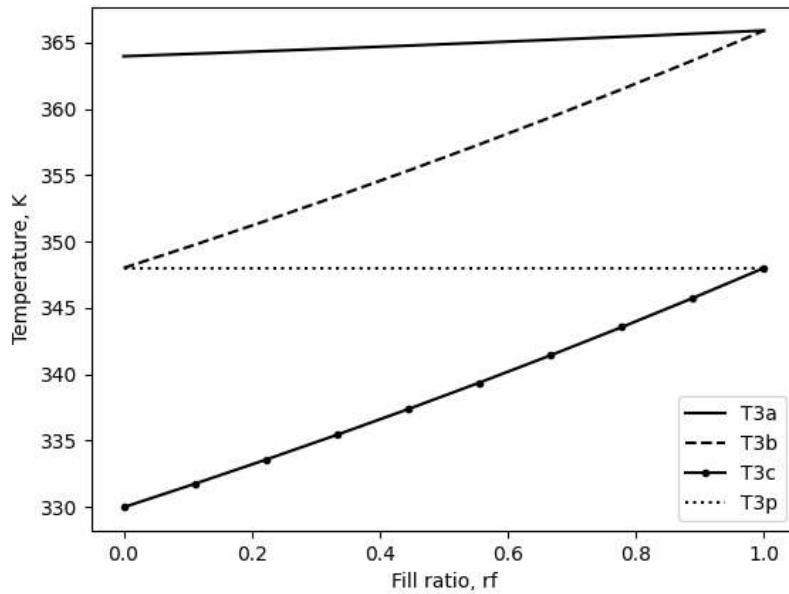


Figure 27: Variation in temperatures (at points p, a, b and c) with fill ratio, at $r_p = 2$ for toluene

For water, instead of increasing temperature after the expansion, T_{3c} , shows a slight decrease and then an increase after a certain fill ratio, r_f , as shown in figure 28. Water being a wet fluid exhibits different behavior for T_{3c} than the fluids examined, which are dry or isentropic. For higher expansion ratios, there is a straight decrease in T_{3c} for water as shown in figure 30 ($T_{hot} = 348K$, $T_{cold} = 293K$, $r_p = 4$).

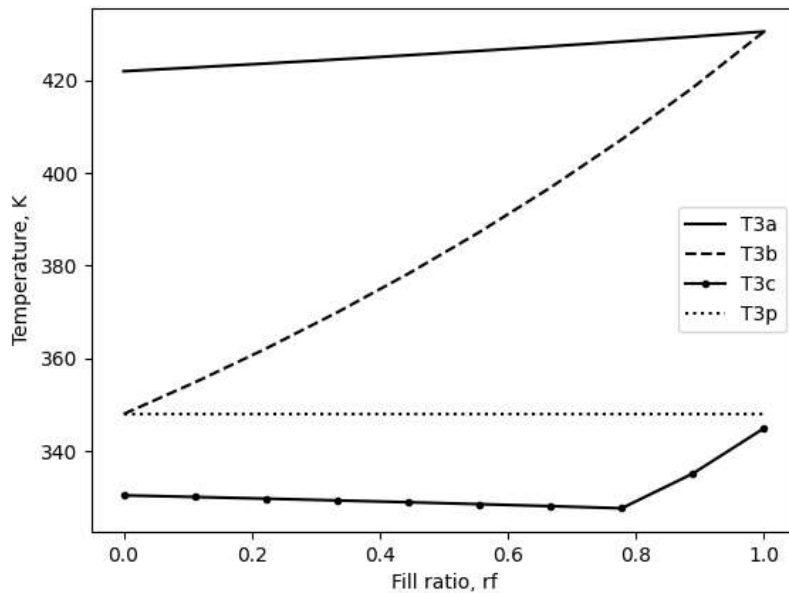


Figure 28: Variation in temperatures (at points p, a, b and c) with fill ratio, at $r_p = 2$ for water

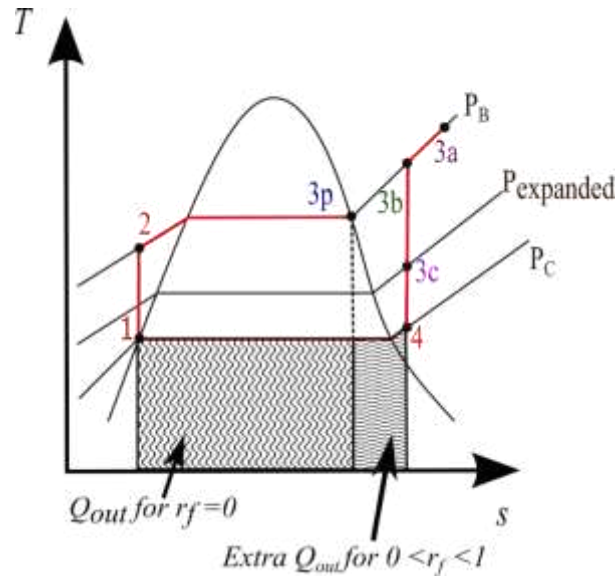


Figure 29: Increase in the area for condenser work under T - s diagram

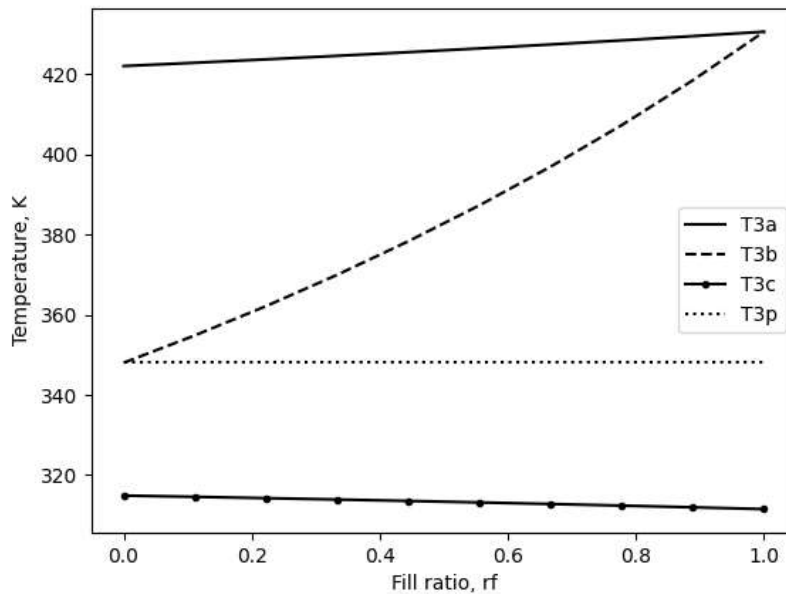


Figure 30: Variation in temperatures (at points p, a, b and c) with fill ratio, at $r_p = 4$ for water

For three of the four substances studied, $r_{p,max}$ does not vary much with r_f as seen in figure 31. For R1234yf, novdec649 and water, $r_{p,max}$ decreases with increasing r_f . R1234yf and novdec649 show a very small decrease, whereas water shows a noticeable decrease. Toluene behaves oppositely, showing a very slight increase with increasing r_f . Water falls under the wet fluid category and due to the slope on T - s curve, shown in figure 32, water shows the above-mentioned behavior. Toluene is a dry fluid, though T - s curve of toluene is a little bit different than that of other dry fluids. The saturated vapor line comes a bit outside for lower temperatures, shown in figure 33.

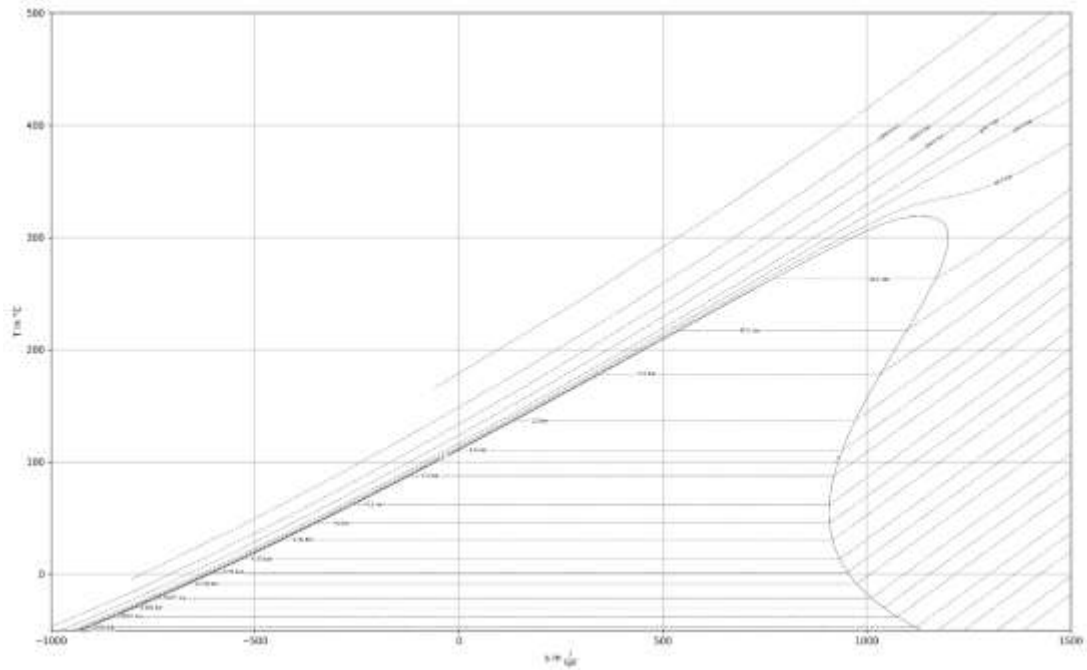


Figure 33: $T - s$ curve, Toluene

4.3 Impact of r_f and r_p on Specific Power

As can be seen from figure 34, specific power decreases with an increase in expansion ratio for all selected fluids. Specific power decreases exponentially for most ranges of r_p , and drops to zero abruptly near $r_{p,max}$. From the selected fluids, R1234yf gives more specific power with small expansion ratios, r_p , which means that using R1234yf smaller engines can be designed with more specific power output, whereas for water and toluene specific power output is very less and engine size becomes large due to larger expansion ratios.

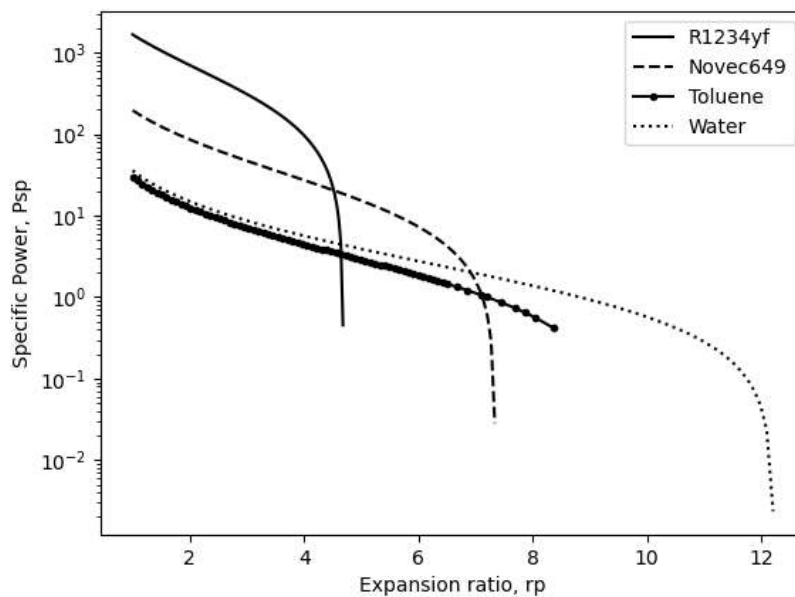


Figure 34: Variation of specific power with expansion ratio at $r_f = 0.1$. The incomplete line for toluene is due to the failure of Brent's method.

Figure 35 shows the variation in efficiency with a specific power. As can be seen from the plot that with the increase in efficiency specific power drops, from which it can be concluded that small devices with high specific power give less efficiency and vice versa. So, to design an efficient system with a good amount of specific power, the selection of r_p should be in between 1 to $r_{p,max}$, according to the requirement.

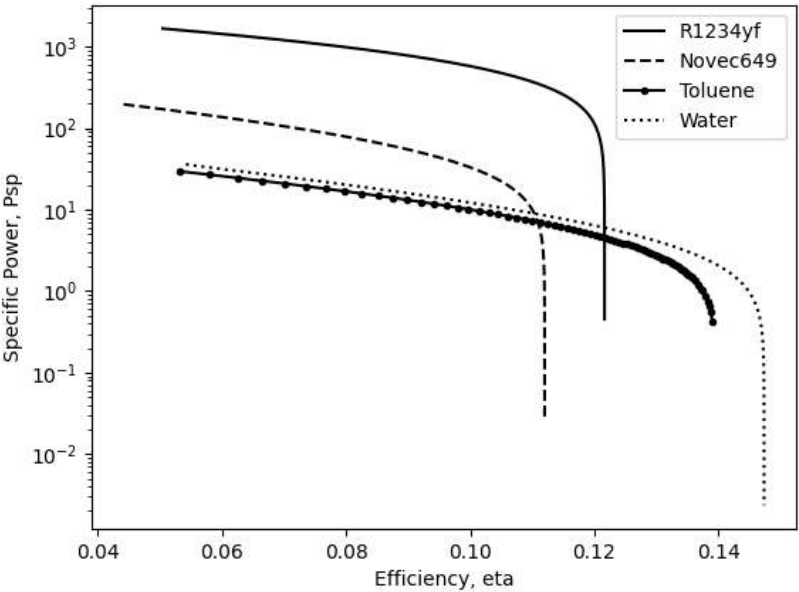


Figure 35: Variation in specific power and Efficiency at $r_f = 0.1$. The incomplete line for toluene is due to the failure of Brent's method.

Fill ratio, r_f has a negative effect on efficiency and the same is true for specific power too, which can be seen from figure 36. But for a given expansion ratio, r_p the negative effect of fill ratio, r_f on specific power is very small. Hence, it can be concluded that for a selected expansion ratio, varying fill ratio, specific power output cannot be changed.

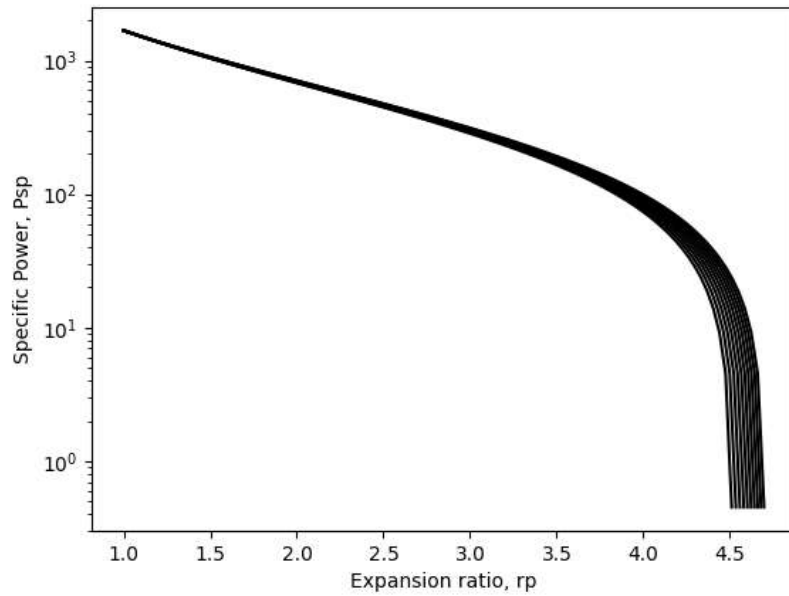


Figure 36: Variation in specific power with expansion ratio for R1234yf at different r_f

Zeta is the ratio of pressure difference achieved by expansion to the maximum pressure difference that can be achieved. From the plot below, figure 37, it is visible that after a certain expansion ratio of each fluid, increasing it further will not result in an increase in work output.

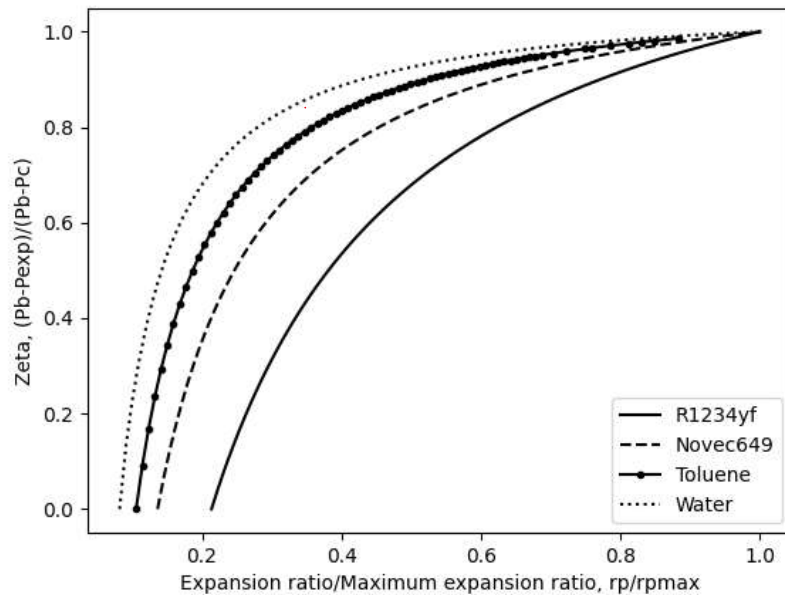


Figure 37: Variation in zeta with $r_p / r_{p,max}$. The incomplete line for toluene is due to the failure of Brent's method.

Fill ratio has a negative effect on efficiency and specific power, but it has almost no impact on zeta, which can be seen in figure 38. Hence, choosing different fill ratios cannot help, increasing work out.

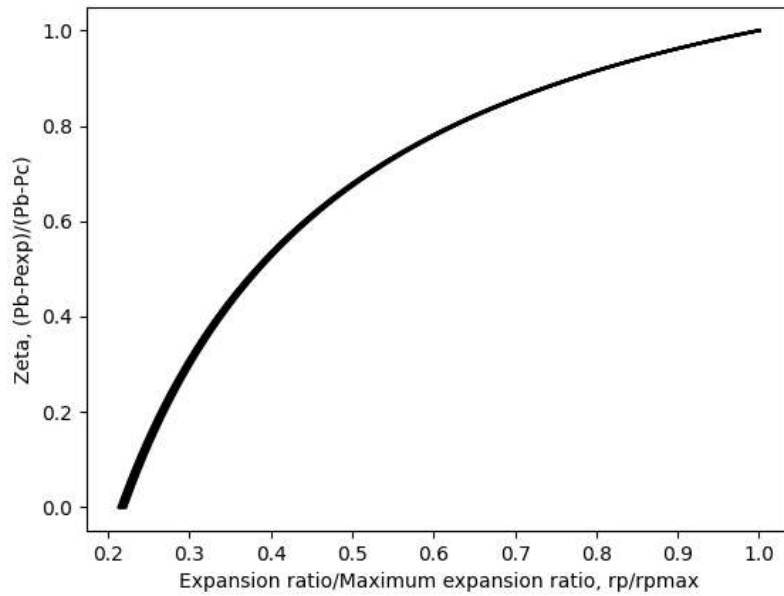


Figure 38: Variation in zeta with $r_p / r_{p,max}$ at different r_f for R1234yf

4.4 Dependence on Hot and Cold Source Temperatures

For a given $T_{cold} = 293K$ and fill ratio, $r_f = 0.1$, the effect of hot source temperature on efficiency at a fixed expansion and fill ratio is studied. For a selected expansion ratio, r_p , Efficiency increases with increasing T_{hot} , reaches a maximum and then drops as can be seen in figures 39 and 40. After reaching maximum efficiency, with the increase in hot source temperature, efficiency starts decreasing. The reason behind that is with a fixed expansion ratio when hot source temperature increases, after a certain value of T_{hot} , the useful energy, which can produce work, is being wasted outside the FPE to reach condenser pressure.

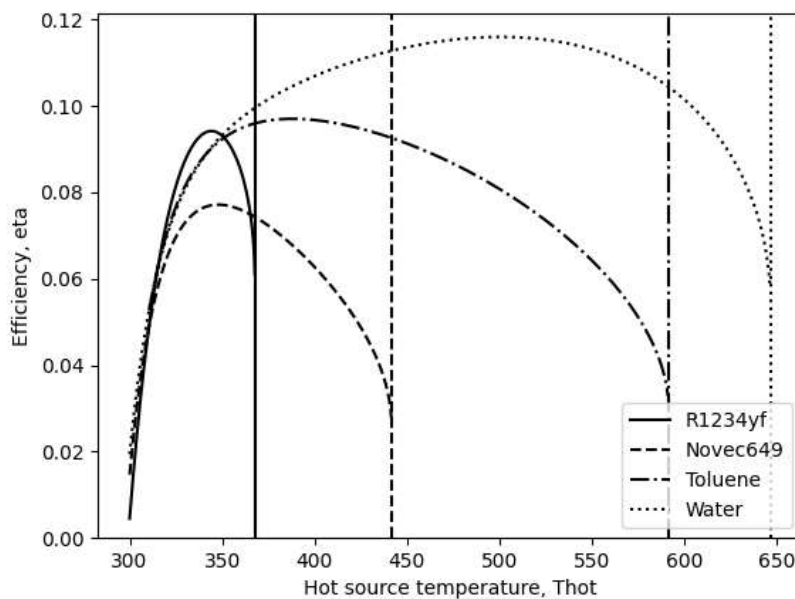


Figure 39: Efficiency vs. hot source temperature at given cold source temperature of 293K at $r_p = 2$.

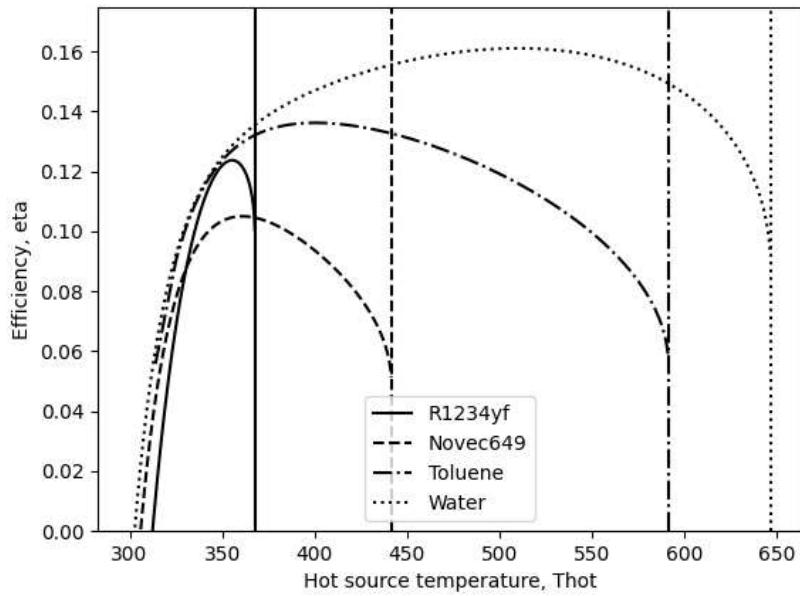


Figure 40: Efficiency vs. hot source temperature at given cold source temperature of 293K at $r_p = 4$.

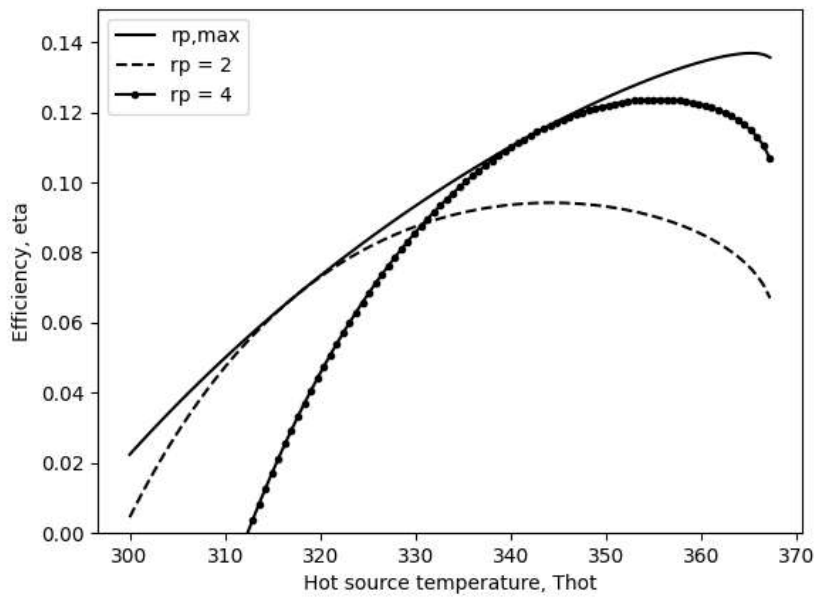


Figure 41: Variation in efficiency with hot source temperature at r_p of 2, 4 and $r_{p,max}$ for R1234yf

The variation of efficiency with hot source temperature is shown in figure 41 for expansion ratios of 2 (--- line) and 4 (- . line). At the hot source temperature, $T_{hot} = 317.3K$, the maximum expansion ratio is 2 and at $T_{hot} = 342.5K$, the maximum expansion ratio is 4. For a hot source temperature below the critical values of $T_{hot} = 317.3K$ ($r_p = 2$) and $T_{hot} = 342.5K$ ($r_p = 4$), the system is in overexpansion and shows an efficiency decrease. The envelope of efficiency at $r_p = r_{p,max}$ is plotted in figure 41(- line) as well.

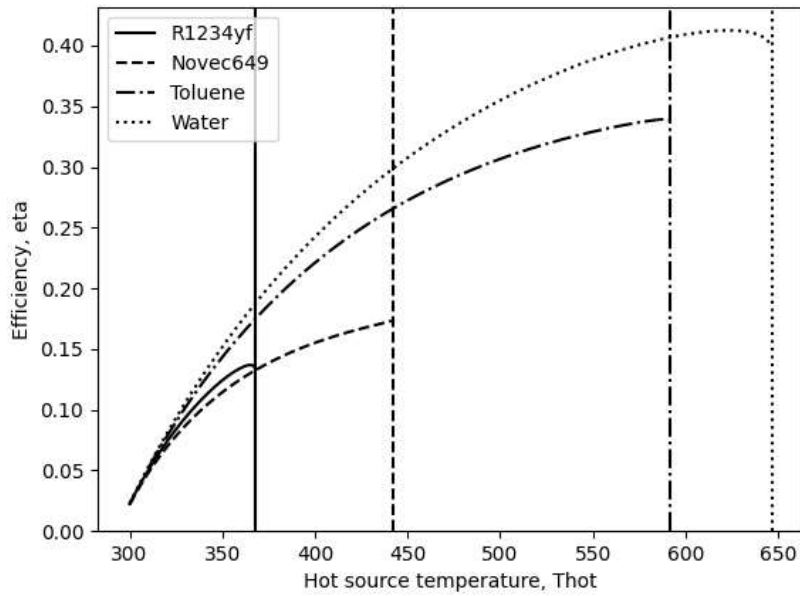


Figure 42: Efficiency vs. hot source temperature at given cold source temperature of 293K at $r_p = r_{p,max}$. The incomplete line for toluene is due to the failure of Brent's method.

For a fixed cold source temperature and fill ratio, when increasing hot source temperature, the maximum achievable expansion ratio varies, increasing exponentially. From figure 43, it can be seen that R1234yf and novsec649 can extract heat at lower temperatures and with small expansion ratios. Water can be used for high temperature (up to 647K) WHR with the maximum possible expansion ratio of 8307.2896.

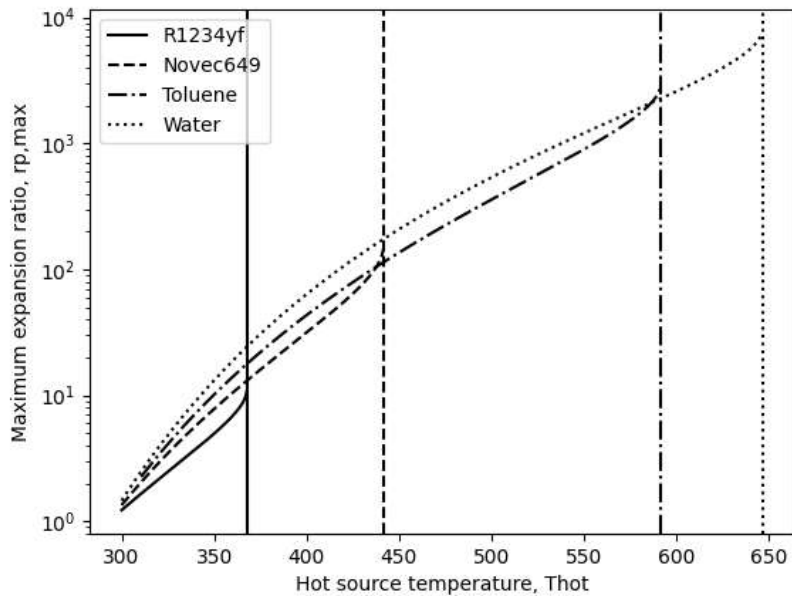


Figure 43: Variation in maximum expansion ratio with a hot source temperature

For a given $T_{hot} = 348K$ and fill ratio, $r_f = 0.1$, efficiency decreases with increasing T_{cold} , which can be seen in figure 44. With the increase in condenser temperature and overall temperature difference of the cycle decreases, reducing operating pressure ranges, hence efficiency. With

increasing expansion ratio, the efficiency drop with cold source temperature, increases which can be noticed in figure 45. For R1234yf efficiency drops by 5%,13.6% and 15.6% for an expansion ratio of 2, 4 and maximum possible expansion ratio, $r_{p,max}$ (which changes with T_{hot} and T_{cold}) respectively, when cold source temperature varies from 290K to 300K.

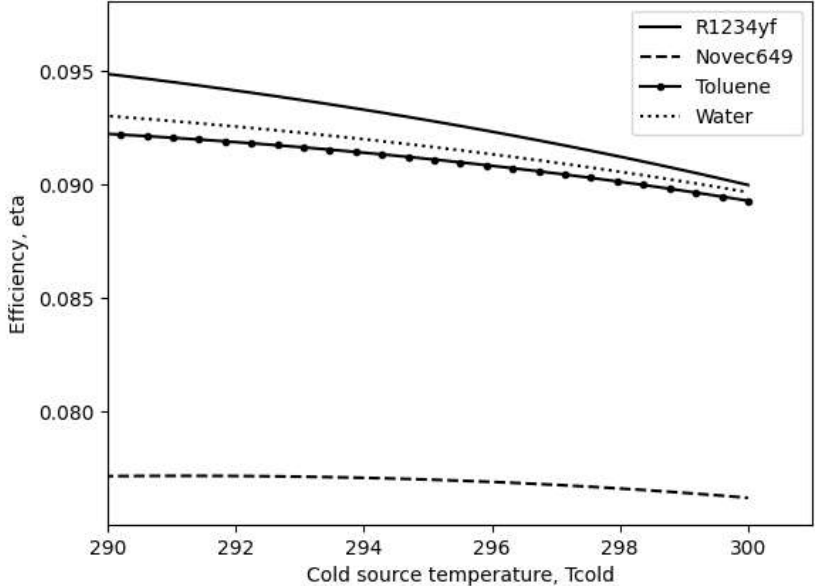


Figure 44: Efficiency vs. cold source temperature at a given hot source temperature of 348K and $r_p = 2$

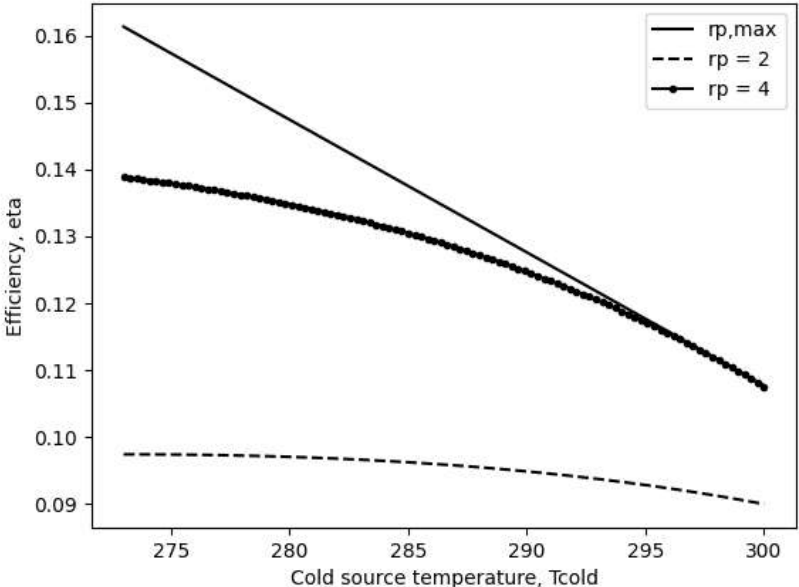


Figure 45: Variation in efficiency with cold source temperature at r_p of 2, 4 and $r_{p,max}$ for R1234yf

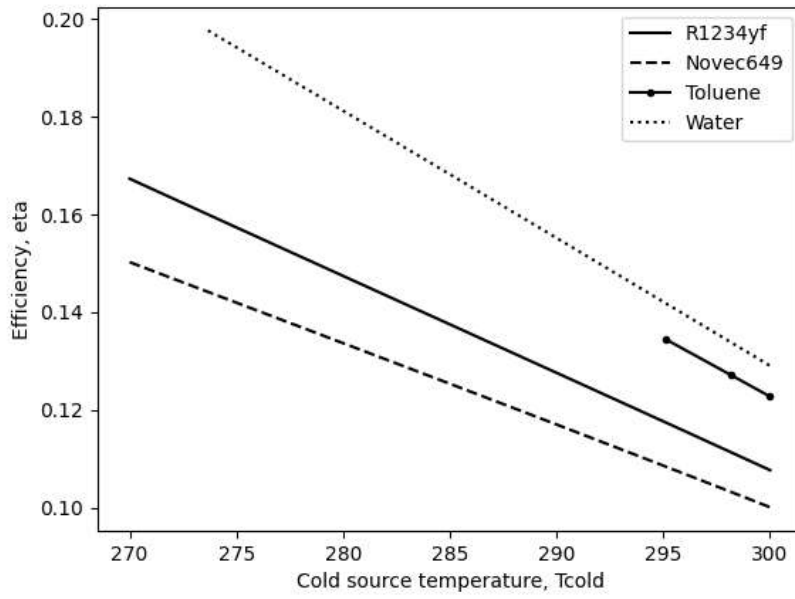


Figure 46: Efficiency vs. cold source temperature at given hot source temperature of 348K at $r_p = r_{p,max}$. The incomplete line for toluene is due to the failure of Brent's method.

5 Case Study for Fluid Selection

For two specific hot source temperatures and two values of maximum piston velocity, the fluid selection process is carried out to design an optimal device. The conditions of the different cases considered are reported in table 3. The value of fill ratio, r_f , is taken as 0.05 to consider the impact of a small volume which is always more than zero in practical use. The optimization function is the efficiency, subject to geometric and environmental constraints. In other words, the maximum efficiency is selected for each fluid that can limit the maximum size of the device. Several possible fluids are reported due to the varied ways in which fluids can impact the environment. The specific procedure and constraints are obtained in section 5.1.

Case	T_{hot} (°C)	T_{cold} (°C)	P_{target} (kW)	r_f	frequency (Hz)	v_{max} (m/s)	η_{carnot} (%)
1	75	20	10	0.05	2	2	15.8
1b	75	20	10	0.05	2	5	15.8
2	200	20	10	0.05	2	2	38.05
2b	200	20	10	0.05	2	5	38.05

Table 3: Set of conditions for case study

5.1 Case 1 and 1b

For the conditions of case 1, the specific power and efficiency are computed for the entire range $r_p = 1$ to $r_p = r_{p,max}$. All 123 fluids in the COOLPROP database are evaluated. The specific power, $P_{sp} = \dot{W}_p/A_p$ is plotted against the thermal efficiency, η .

The fluids are picked for which P_{sp} can reach between 150 kW/m² and 200 kW/m². The reason behind selecting the above-mentioned values of P_{sp} is to keep the piston diameter in the range of 3 to 12 inches. For a target power output of 10kW and $D_p = 12$ inches, $P_{sp} = 141$ kW/m². For a target power output of 1kW and $D_p = 3$ inches, $P_{sp} = 220$ kW/m². For a particular fluid, the specific power is maximum at $r_p = 1$, however, the efficiency is minimum at that point. The efficiency is maximized at $r_p = r_{p,max}$, however, the specific power tends to zero. For high expansion ratios, efficiency is nearly constant, whereas, for low expansion ratios, the specific power remains very high, giving the general L-shape of the relationship shown in figure 47. For each fluid, r_p is selected which intersects the line $P_{sp} = 150$ kW/m². However, if the knee of the curve is above the threshold, an expansion ratio is selected to maximize P_{sp} with a tolerable efficiency loss. Corresponding to the picked r_p value, for a fixed power output of 10kW, piston diameter and length, condenser pressure, boiler pressure, and expansion pressure is calculated. Finally, the fluid toxicity, availability, and usability are considered to reject problematic fluid. The final fluid list and corresponding parameters are reported in table 4 in appendix B.

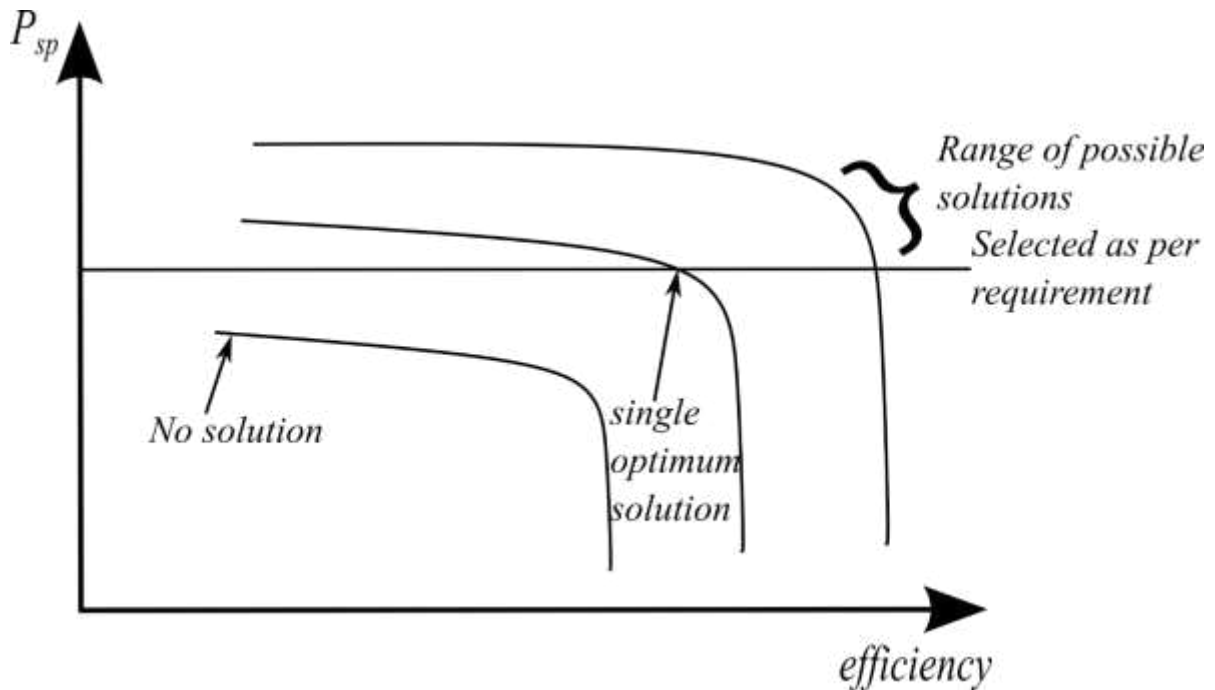


Figure 47: Specific power vs. efficiency curve for fluid selection

For case 1, to produce 10kW of power suitable fluids are Ammonia, R1234ze(Z), R1234ze(E), R1234yf, R1233zd(E) and novoc649 with an efficiency of 0.1368, 0.1219, 0.1213, 0.1191, 0.1141 and 0.0790 respectively. To use these fluids there are certain safety measures (listed in table 4) that need to be taken in order to operate safely.

For the conditions of case 1b, following the same procedure, the specific power and efficiency are computed for the entire range $r_p = 1$ to $r_p = r_{p,max}$. All 123 fluids in the COOLPROP database are evaluated. The final fluid list and corresponding parameters are obtained and reported in table 5 in appendix B. To produce 10kW of power the suitable fluids are the same: Ammonia, R1234ze(Z), R1233zd(E), R1234ze(E), R1234yf and novoc649. The efficiency is 0.1386, 0.1307, 0.1304, 0.1260, 0.1215 and 0.1036 respectively.

From case 1 and 1b, it is visible that the maximum allowable piston velocity has a large impact on the total piston length as seen in Tables 4 and 5. Increasing velocity increases the piston length and, therefore, for 1b the piston length to diameter ratio is more than that for case 1.

5.2 Case 2 and 2b

For case 2 and 2b, following the same procedure mentioned in section 5.1, the specific power and efficiency are computed for the entire range r_p from 1 to $r_{p,max}$. All fluids are evaluated.

There exist a much smaller number of fluids that can be used at the higher temperature of case 2. This is due to the requirement of saturated vapor boiler output, thus requiring $T_{critical} > T_{hot}$. Allowing superheated output would yield more options. All the identified fluids are toxic, flammable, banned, or have high ODP and GWP except water, making it the one and only choice for the constraints considered. It gives an efficiency of 0.2485 despite the piston diameter being larger (14.07 inches) than the length (3.75 inches).

For case 2b, again, the only usable fluid is water with nearly the same efficiency as in case 2, but the aspect ratio (length to diameter) is 1.05 with 8.90 inches diameter and 9.38 inches length. The results of the fluid selection of cases 2 and 2b is in table 6 and 7 in appendix B.

From all cases studied, it can be concluded that increasing the hot source temperature, T_{hot} increases the workable expansion ratio (see section 4.4). At the same time, limits the choice of working fluids. For lower piston velocities of order 2-5 m/s, the FPE is mostly square-shaped with large piston diameters.

6 Conclusion and Future Work

A model was formulated that includes the entropy and temperature rise associated with the rapid filling of the dead volume, captured by the fill ratio. The expansion ratio is constrained by the maximum piston velocity and frequency for fixed power output. The design of an FPE is carried out with the given constraints, which are used to predict physical dimensions and efficiency for different fluids. The initial selection of fluid is based on environmental impact and safety considerations. Afterward, based on the space availability, a fluid is selected to reach maximum efficiency. The designed model may have a significant effect on the environment as it recaptures and reutilizes the waste heat to produce useful work.

The two main parameters affecting cycle performance are the expansion ratio and fill ratio. Increasing the expansion ratio increases efficiency up to a certain level, while simultaneously decreasing the specific power output. Increasing fill ratio, on the other hand, has a negative impact on both efficiency and power output. With a surge in hot source temperature, the maximum possible expansion ratio increases. The efficiency shoots up, reaches a maximum, and drops off with increasing hot source temperature, while it rationally decreases with increasing cold source temperature. For designing an efficient cycle, the fill ratio should be minimum with a selected optimum expansion ratio at which specific power and FPE dimensions match the requirements for maximum possible efficiency. There is a suitable working fluid for the given application and with the change in operating parameters (r_f , r_p , T_{hot} , T_{cold}), it changes. A rise in maximum possible piston velocity increases the expansion ratios and, length to diameter ratio of FPE. Hot source temperature increase limits the choice of fluid.

Boiler output is fixed as a saturated vapor and hence the choice of fluids is limited at high hot source temperatures. A separate study can be done by allowing superheated boiler output for optimization. Using two or more FPE in series for minimizing energy loss can be studied to optimize the configuration and fluid selection.

7 Bibliography

- [1] "Fossil fuel consumption, World," [Online]. Available: <https://ourworldindata.org/grapher/fossil-fuel-consumption-by-type>.
- [2] K. Gioietta, "When Fossil Fuels Run Out, What Then?," [Online]. Available: <https://mahb.stanford.edu/library-item/fossil-fuels-run/>.
- [3] E. H. Wang, H. G. Zhang, B. Y. Fan, M. G. Ouyang, Y. Zhao, Q. H. Mu, "Study of Working Fluid Selection of Organic Rankine Cycle (ORC) for Engine Waste Heat Recovery," *Energy*, vol. 36, no. 5, p. 3406 – 3418, May 2011.
- [4] L. Baker, "Combined heat and power cogeneration can ensure consistency and save energy," December 2019. [Online]. Available: <https://www.foodengineeringmag.com/articles/98624-combined-heat-and-power-cogeneration-can-ensure-consistency-and-save-energy>.
- [5] "WASTE HEAT TO POWER SYSTEMS," United States Environmental Protection Agency, [Online]. Available: https://www.epa.gov/sites/default/files/2015-07/documents/waste_heat_to_power_systems.pdf.
- [6] H. Jouhara, N. Khordehgah, S. Almahmoud, B. Delpech, A. Chauhan, S. A. Tassou, "Waste Heat Recovery Technologies and Applications," *Thermal Science and Engineering progress*, vol. 6, p. 268 - 289, June 2018.
- [7] V. Zare, S. M. S. Mahmoudi, "A Thermodynamic Comparison between Organic Rankine and Kalina cycles for Waste Heat Recovery from the Gas Turbine - Modular Helium Reactor," *Energy*, vol. 79, p. 398 - 406, January 2015.
- [8] X. Hou, H. Zhang, F. Yu, H. Liu, F. Yang, Y. Xu, Y. Tian, G. Li, "Free Piston Expander-Linear Generator Used for Organic Rankine Cycle Waste Heat Recovery System," *Applied Energy*, vol. 208, p. 1297 – 1307, December 2017.
- [9] S. Saghatoun, W. Zhuge, Y. Zhang, "Review of Expander Selection for Small-Scale Organic Rankine Cycle," *American Society of Mechanical Engineers*, vol. 1, no. B, 2014.
- [10] O. Dumont, A. Parthoens, R. Dickes, V. Lemort, "Experimental Investigation and Optimal Performance Assessment of Four Volumetric Expanders (Scroll, Screw, Piston and Roots) Tested in a Small-Scale Organic Rankine Cycle System," *Energy*, vol. 165, p. 1119 - 1127, December 2018.
- [11] F. Alshammari, U. Muhammad, A. Pesyridis, "Expanders for Organic Rankine Cycle Technology," in *Organic Rankine Cycle Technology for Heat Recovery*, E. Wang, Ed., InTech, 2018.
- [12] F. Heberle, M. Preißinger, D. Brüggemann, "Zeotropic Mixtures as Working Fluids in Organic Rankine Cycles for Low-Enthalpy Geothermal Resources," *Renewable Energy*, vol. 37, no. 1, p. 364 – 370, January 2012.
- [13] J. Bao, L. Zhao, "A Review of Working Fluid and Expander Selections for Organic Rankine Cycle," *Renewable and Sustainable Energy Reviews*, vol. 24, p. 325 – 342, August 2013.
- [14] C. He, C. Liu, H. Gao, H. Xie, Y. Li, S. Wu, J. Xu, "The Optimal Evaporation Temperature and Working Fluids for Subcritical Organic Rankine Cycle," *Energy*, vol. 38, no. 1, p. 136 – 143, February 2012.

- [15] S. Gequn, Y. Gao, H. Tian, H. Wei, X. Liang, "Study of Mixtures Based on Hydrocarbons Used in ORC (Organic Rankine Cycle) for Engine Waste Heat Recovery," *Energy*, vol. 74, p. 428 – 438, September 2014.
- [16] Y. Lu, A. P. Roskilly, L. Jiang, L. Chen, Y. Xiaoli, "Analysis of a 1 KW Organic Rankine Cycle Using a Scroll Expander for Engine Coolant and Exhaust Heat Recovery," *Frontiers in Energy*, vol. 11, no. 4, p. 527 – 534, December 2017.
- [17] Y. A. Cengel, M. A. Boles, *Thermodynamics: An engineering approach*, McGraw Hill, 2008.
- [18] X. Zhang, M. He, Y. Zhang, "A Review of Research on the Kalina Cycle," *Renewable and Sustainable Energy Reviews*, vol. 16, no. 7, p. 5309 – 5318, September 2012.
- [19] A. F. Babatunde, O. O. Sunday, "A Review of Working Fluids for Organic Rankine Cycle (ORC) Applications," in *IOP Conference Series: Materials Science and Engineering*, September 10, 2018.
- [20] Z. Li, L. Yiji, H. Yuqi, Q. Gao, C. Fenfang, Y. Xiaoli, A. Roskilly, "Comparison Study of Trilateral Rankine Cycle, Organic Flash Cycle and Basic Organic Rankine Cycle for Low Grade Heat Recovery," in *Energy Procedia*, 2017.
- [21] M. Yari, A. S. Mehr, V. Zare, S. M. S. Mahmoudi, M. A. Rosen, "Exergoeconomic Comparison of TLC (Trilateral Rankine Cycle), ORC (Organic Rankine Cycle) and Kalina Cycle Using a Low Grade Heat Source," *Energy*, vol. 83, p. 712 - 722, April 2015.
- [22] G. Persico, M. Pini, "Fluid Dynamic Design of Organic Rankine Cycle Turbines," in *Organic Rankine Cycle (ORC) Power systems*, Woodhead Publishing, 2017, p. 253 – 297.
- [23] S. Emhardt, G. Tian, J. Chew, "A Review of Scroll Expander Geometries and Their Performance," *Applied Thermal Engineering*, vol. 141, p. 1020 – 1034, August 2018.
- [24] B. Peng, B. Zhu, V. Lemort, "Theoretical and Experimental Analysis of Scroll Expander," in *International Compressor Engineering Conference*, 2016.
- [25] J.F. Oudkerk, R. Dickes, O. Dumont, V. Lemort, "Experimental Performance of a Piston Expander in a Small- Scale Organic Rankine Cycle," in *IOP Conference Series: Materials Science and Engineering*, August 10, 2015.
- [26] M. Imran, M. Usman, "Mathematical Modelling for Positive Displacement Expanders," in *Positive Displacement Machines*, Academic Press, 2019, p. 293 – 343.
- [27] Y. Wang, L. Chen, B. Jia, A. P. Roskilly, "Experimental Study of the Operation Characteristics of an Air-Driven Free-Piston Linear Expander," *Applied Energy*, vol. 195, p. 93 – 99, June 2017.
- [28] S. Douvartzides, I. Karmalis, "Working Fluid Selection for the Organic Rankine Cycle (ORC) Exhaust Heat Recovery of an Internal Combustion Engine Power Plant," in *IOP Conference Series: Materials Science and Engineering*, November 2016.
- [29] "How do CFCs destroy the ozone layer?," [Online]. Available: <https://www.lifegate.com/how-cfcs-destroy-ozone-layer>.
- [30] A. Benzaoui, S. Benhadid-Dib, "Refrigerants and their Environmental Impact Substitution of Hydro Chlorofluorocarbon HCFC and HFC Hydro Fluorocarbon. Search for an Adequate Refrigerant," *Energy Procedia*, vol. 18, p. 807 - 816, 2012.
- [31] "Chlorofluorocarbons (CFCs) and hydrofluorocarbons (HFCs)," [Online]. Available: <https://www.pca.state.mn.us/air/chlorofluorocarbons-cfcs-and-hydrofluorocarbons-hfcs>.
- [32] "The Vienna Convention for the Protection of the Ozone Layer," [Online]. Available: <https://ozone.unep.org/treaties/vienna-convention>.

- [33] "Vienna Convention and the Montreal Protocol," [Online]. Available: <https://www.bafu.admin.ch/bafu/en/home/topics/chemicals/info-specialists/international-affairs--chemicals/vienna-convention-and-the-montreal-protocol.html>.
- [34] "Kigali Amendment," [Online]. Available: https://en.wikipedia.org/wiki/Kigali_Amendment.
- [35] "Kyoto Protocol," [Online]. Available: https://en.wikipedia.org/wiki/Kyoto_Protocol#Background.
- [36] R. W. James, T. C. Welch, "Refrigeration and Heat-Pump Systems," in *Air Conditioning System Design*, 2017, p. 167 – 189.
- [37] J. M. Rodriguez, Treatise on Geochemistry, K. K. T. Heinrich D. Holland, Ed., Pergamon, 2007, p. 1-34.
- [38] L. M. Amoo, R. L. Fagbenle, "15 - Climate change in developing nations of the world," in *Applications of Heat, Mass and Fluid Boundary Layers*, O. A. S. A. A. F. R.O. Fagbenle, Ed., Woodhead Publishing, 2020, p. 437- 471.
- [39] Madhu, "Difference Between Azeotropic and Zeotropic Mixture," [Online]. Available: <https://www.differencebetween.com/difference-between-azeotropic-and-zeotropic-mixture/>.
- [40] C. Kuo, H. Sung-Wei, K. Chang, C. Wang, "Analysis of a 50kW Organic Rankine Cycle System," *Energy*, vol. 36, no. 10, p. 5877 – 5885, October 2011.
- [41] Y. Tian, H. Zhang, L. Jian, H. Xiaochen, T. Zhao, F. Yang, X. Yonghong, X. Wang, "Development and Validation of a Single-Piston Free Piston Expander-Linear Generator for a Small-Scale Organic Rankine Cycle," *Energy*, vol. 161, p. 809 - 820, October 2018.
- [42] G. Li, H. Zhang, F. Yang, S. Song, Y. Chang, F. Yu, J. Wang, B. Yao, "Preliminary Development of a Free Piston Expander–Linear Generator for Small-Scale Organic Rankine Cycle (ORC) Waste Heat Recovery System," *Energies*, vol. 9, no. 4, p. 300, 20 April 2016.
- [43] X. Hou, H. Zhang, Y. Xu, Y. Tian, T. Zhao, J. Li, F. Yu, "Performance Investigation of a Free Piston Expander-Linear Generator for Small Scale Organic Rankine Cycle," *Applied Thermal Engineering*, vol. 144, p. 209 - 218, November 2018.
- [44] S. Preetham Burugupally, L. Weiss, "Design and Performance of a Miniature Free Piston Expander," *Energy*, vol. 170, p. 611 – 618, March 2019.
- [45] C. Champagne, L. Weiss, "Performance Analysis of a Miniature Free Piston Expander for Waste Heat Energy Harvesting," *Energy Conversion and Management*, vol. 76, p. 883 – 892, December 2013.
- [46] B.S. Preetham, L. Weiss., "Investigations of a New Free Piston Expander Engine Cycle," *Energy*, vol. 106, p. 535 – 545, July 2016.
- [47] "List of refrigerants," [Online]. Available: https://en.wikipedia.org/wiki/List_of_refrigerants.
- [48] "What is the phase-out schedule for HCFC refrigerants?," [Online]. Available: <https://www.ashrae.org/File%20Library/Technical%20Resources/Technical%20FAQs/TC-02.05-FAQ-33.pdf>.

Appendix A: *T-s* curves for the fluids Novec649 and R1234yf

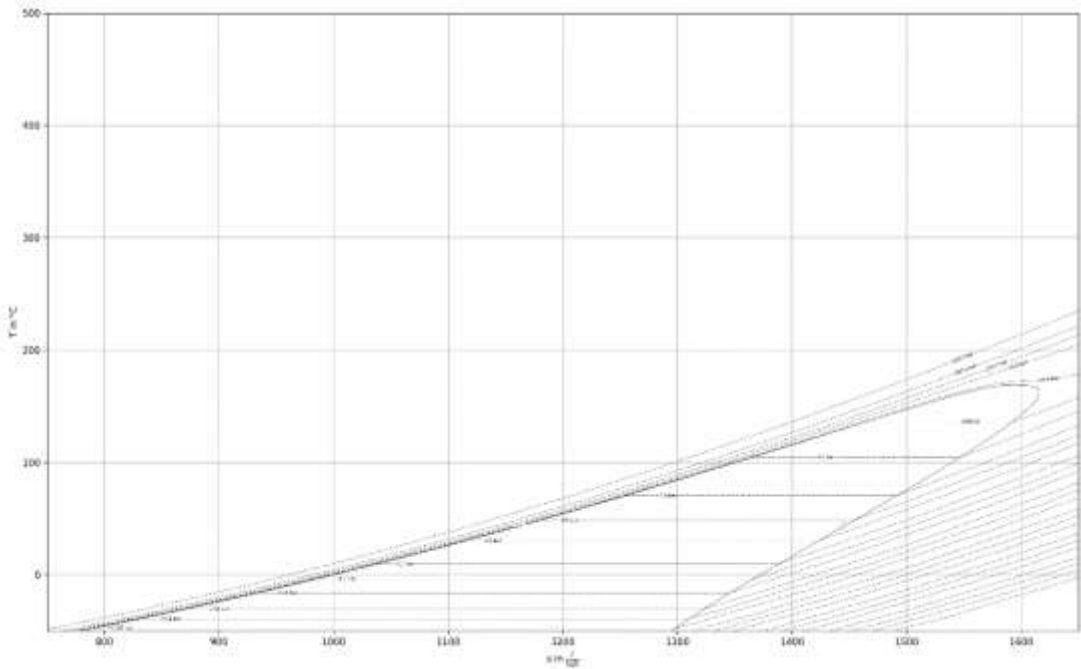


Figure 48: *T-s* curve, Novec649

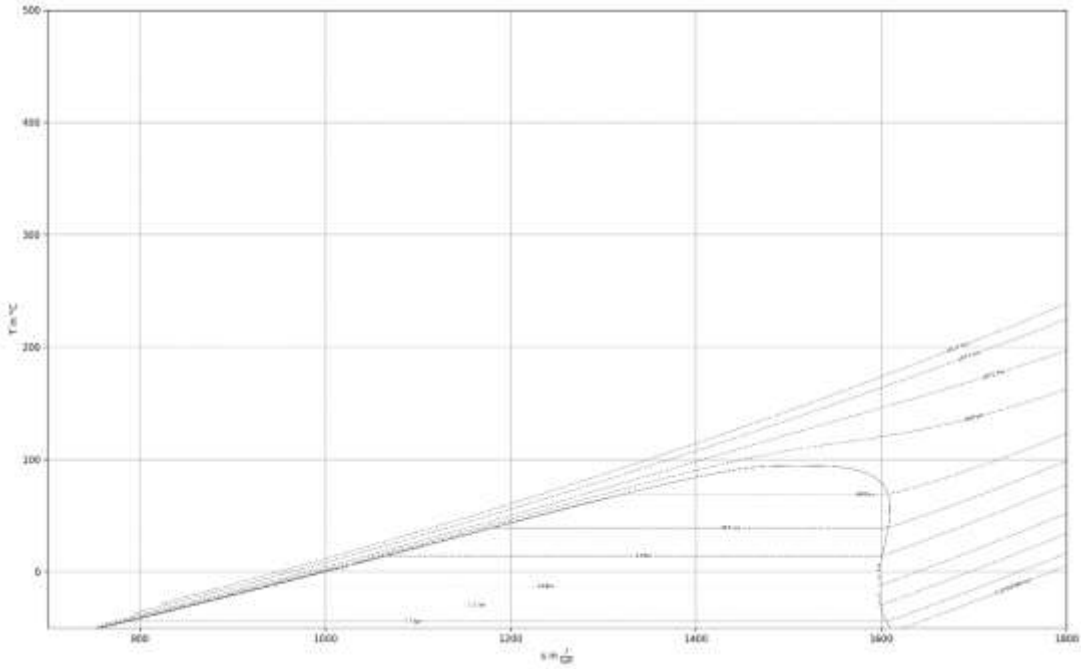


Figure 49: *T-s* curve, R1234yf

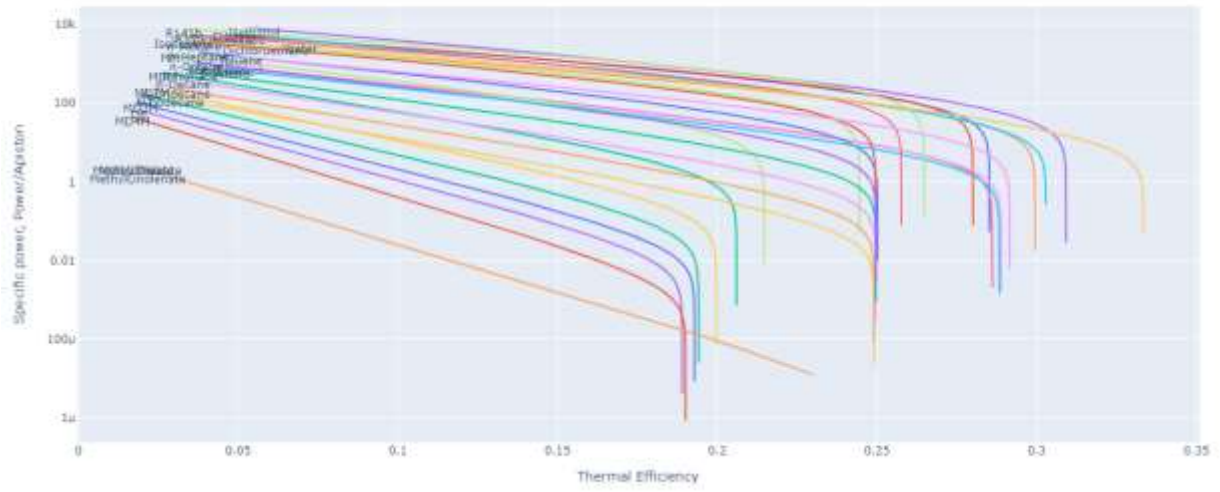


Figure 52: P_{sp} vs. efficiency at different expansion ratios for all fluids in COOLPROP for case 2

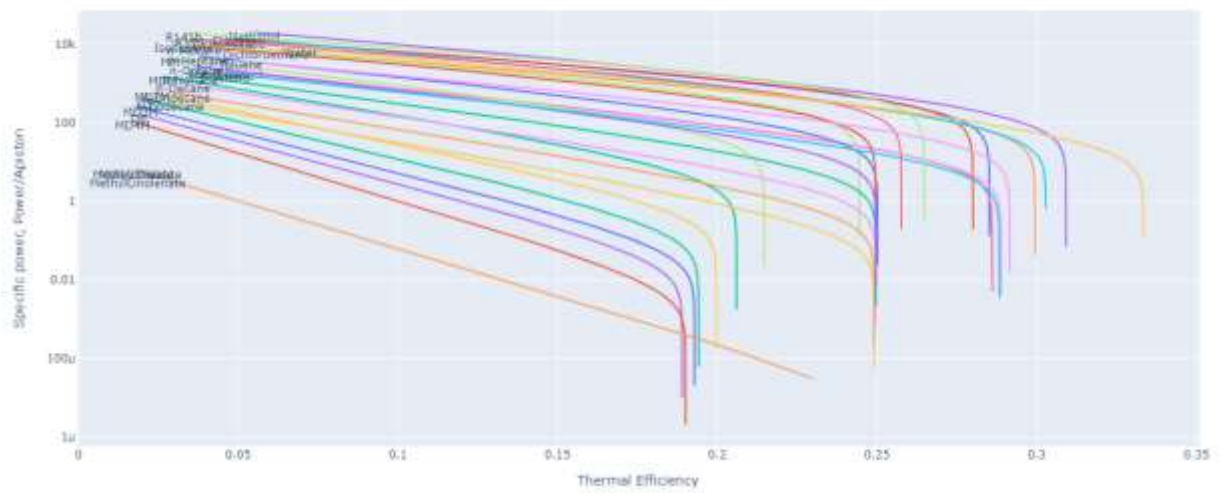


Figure 53: P_{sp} vs. efficiency at different expansion ratios for all fluids in COOLPROP for case 2b

Appendix C: Possible fluids for the case studies

Fluid	r_p	P_{sp} (kW / m ²)	Efficiency	D_p (in)	L_{Total} (in)	P_C (bar)	P_B (bar)	$P_{expanded}$ (bar)	Useable?	Reason
Ammonia	3	526.29	0.1368	6.12	3.23	8.57	37.10	11.20	Y	Corrosive, Acute toxic, environment hazard
Sulfur Dioxide	2.7	402.12	0.1332	7.01	5.06	3.31	16.01	5.32	N	Skin corrosive, toxic if inhaled
Cyclopropane	2.7	429.09	0.1311	6.78	4.13	6.32	22.93	8.46	N	Extremely flammable
Carbonyl Sulfide	2.5	670.92	0.1307	5.42	4.03	11.30	37.23	14.65	N	Flammable, Acute toxic, Irritant, Compressed gas
Hydrogen Sulfide	2.4	1138.39	0.1301	4.16	4.32	17.81	57.97	23.50	N	Flammable, Acute toxic, Environment hazard
Dimethyl Ether	2.9	365.14	0.1298	7.35	4.05	5.10	20.10	6.92	N	Flammable
Ethylene Oxide	2.5	263.61	0.1294	8.65	6.37	1.45	7.65	2.77	N	Flammable, Acute toxic, Health hazard, Carcinogenicity
Propyne	2.5	584.20	0.1283	5.81	5.79	5.03	20.18	7.95	N	Flammable, Compressed gas, Irritant
R21	2.5	260.07	0.1268	8.71	6.39	1.53	7.61	2.83	N	Phased out under Montreal Protocol
R12	2.9	373.46	0.1267	7.27	4.08	5.66	20.81	7.53	N	Phased out under Montreal Protocol
R161	2.9	541.26	0.1262	6.04	4.13	8.05	29.70	10.75	N	Extremely Flammable, Compressed gas, GWP:4
1-Butene	2.8	276.67	0.1262	8.45	5.34	2.55	10.73	3.93	N	Extremely Flammable, Compressed gas

R152A	2.9	469.15	0.1260	6.49	4.80	5.13	21.05	7.47	N	Extremely Flammable, ODP:0, GWP:124, AL:1.4 years
R142b	2.8	319.06	0.1256	7.86	5.34	2.89	12.38	4.48	N	Production is banned under Montreal protocol (Kigali amendment) from January 1, 2020
R131I	2.5	457.51	0.1255	6.57	5.72	4.26	16.26	6.55	N	Health hazard, Germ cell mutagenicity
Iso Butene	2.8	284.16	0.1254	8.33	5.36	2.61	10.99	4.03	N	Extremely Flammable, Explosive
n-Butane	2.9	228.31	0.1250	9.30	5.26	2.08	9.06	3.22	N	Extremely Flammable, Compressed gas
cis-2-Butene	2.5	291.39	0.1234	8.23	6.62	1.81	8.31	3.27	N	Extremely Flammable, Compressed gas
HFE143m	3.4	345.66	0.1229	7.56	4.04	4.95	19.95	6.68	N	Irritant, Compressed gas, explode if heated
Iso Butane	2.8	318.97	0.1228	7.87	5.49	3.02	12.11	4.62	N	Extremely Flammable, Explosive
n-Propane	2.9	534.35	0.1225	6.08	4.32	8.36	28.49	11.04	N	Extremely Flammable
trans-2-Butene	2.5	313.60	0.1223	7.93	6.69	1.99	8.89	3.56	N	Extremely Flammable, Compressed gas
R124	3	351.66	0.1219	7.49	5.28	3.27	14.13	5.03	N	GWP:527, AL:5.8 years
R1234ze(Z)	2.8	249.20	0.1219	8.90	6.32	1.49	7.61	2.73	Y (A2L safety level)	Lower Flammability and toxicity
Propylene	2.8	649.09	0.1217	5.51	4.40	10.17	33.88	13.42	N	Extremely Flammable, Compressed gas, Environment hazard
R1234ze(E)	3.2	392.06	0.1213	7.09	4.82	4.27	18.01	6.23	Y (A2L safety level)	Lower Flammability and toxicity
R236EA	3.4	203.90	0.1208	9.84	4.97	1.72	8.88	2.74	N	GWP:1330, AL:10.7 years

R1243zf	3	467.95	0.1205	6.49	5.14	5.10	19.88	7.44	N	Flammable, Compressed gas
R134a	3.1	547.96	0.1204	6.00	5.05	5.72	23.64	8.46	N	Banned under Montreal protocol (Kigali amendment)
R236FA	3.4	259.81	0.1195	8.72	5.08	2.29	11.09	3.59	N	Compressed gas, Irritant, Asphyxiant
R245fa	3	222.35	0.1193	9.42	6.24	1.23	6.95	2.34	N	Non-toxic, simple asphyxiant, ODP:0, GWP:858, AL:7.6 years
R1234yf	3.5	383.52	0.1191	7.17	4.04	5.92	22.72	7.83	Y (with proper air conditioning)	Lightly Flammable
R32	3.5	731.62	0.1190	5.19	3.34	14.75	54.17	18.40	N	Flammable, ODP:0, GWP:677, AL:4.9 years
R11	2.2	221.14	0.1188	9.45	8.11	0.89	4.63	1.99	N	Phased out under Montreal protocol
R141b	2.4	165.75	0.1186	10.91	7.71	0.65	3.71	1.48	N	Banned under Montreal protocol
R227EA	3.8	278.57	0.1165	8.42	4.02	3.89	16.65	5.28	N	Compressed gas, ODP:0, GWP:3220, AL:31-42 years
Neopentane	2.6	231.69	0.1165	9.23	6.73	1.46	6.59	2.62	N	Extremely Flammable, Environment hazard
R1233zd(E)	2.4	267.59	0.1141	8.59	7.98	1.08	5.81	2.42	Y	Non-flammable, ODP:0, GWP:1, AL:0.07123 years
R245ca	2.6	219.83	0.1126	9.47	7.69	0.82	5.01	1.92	N	GWP:76, AL:6.2 years
RC318	3.3	301.56	0.1117	8.09	5.41	2.66	12.00	4.16	N	Compressed gas, Environment hazard, GWP:10300, AL:3200 years
Diethyl Ether	2.4	173.77	0.1110	10.66	8.29	0.59	3.53	1.46	N	Extremely Flammable, Irritant

R123	2.2	234.68	0.1105	9.17	8.89	0.76	4.30	1.93	N	ODP:0.012, GWP:76, Listed in phase out schedule (no more production but can be recycled and used till 2030)
R115	3.9	522.12	0.1099	6.15	4.54	7.91	28.22	10.52	N	Phased out under Montreal protocol
Isopentane	2.2	215.37	0.1093	9.57	8.83	0.77	4.05	1.84	N	Extremely Flammable and Volatile, Irritant, Health and Environment hazard
Cyclopentane	2	141.82	0.1086	11.80	9.83	0.35	2.20	1.06	N	Flammable
R113	2.1	145.42	0.1043	11.65	9.71	0.37	2.32	1.09	N	Phased out under Montreal protocol
Acetone	1.9	136.55	0.1029	12.02	10.60	0.25	1.86	0.93	N	Flammable, Irritant
R365MFC	2.2	186.95	0.1008	10.27	9.53	0.46	3.06	1.40	N	GWP:804, AL:8.6 years
Methanol	1.9	122.24	0.0973	12.71	11.01	0.13	1.51	0.74	N	Flammable, Acute toxic (oral, dermal, inhalation), Health hazard
n-Hexane	1.7	113.57	0.0863	13.18	12.53	0.16	1.23	0.73	N	Highly Flammable and Explosive
Iso hexane	1.6	150.36	0.0857	11.46	12.90	0.23	1.59	0.98	N	Flammable, Hazardous
Novec649	2	173.01	0.0790	10.68	10.98	0.33	2.30	1.19	Y	Non-flammable, ODP:0, GWP:1, AL:0.014 years

Table 4: Fluid list and corresponding parameters for case 1; ODP & GWP data [47]

Fluid	r_p	P_{sp} (kW / m ²)	Efficiency	D_p (in)	L_{Total} (in)	P_C (bar)	P_B (bar)	$P_{expanded}$ (bar)	Useable?	Reason
Ethylene Oxide	3.4	255.41	0.1392	8.79	7.76	1.45	7.65	1.96	N	Flammable, Acute toxic Irritant, Health hazard, Carcinogenicity
Sulfur Dioxide	3.3	470.27	0.1387	6.48	6.93	3.31	16.01	4.25	N	Skin corrosive, toxic if inhaled
Ammonia	3.3	754.10	0.1386	5.12	5.02	8.57	37.10	10.08	Y	Corrosive, Acute toxic, Environment hazard
R21	3.3	278.42	0.1358	8.42	8.39	1.53	7.61	2.09	N	Phased out under Montreal protocol
Propyne	3.2	543.84	0.1354	6.02	6.52	5.03	20.18	6.12	N	Flammable, Compressed gas, Irritant
Cyclopropane	3	577.63	0.1338	5.85	6.12	6.32	22.93	7.47	N	Extremely Flammable
Hydrogen Sulfide	2.8	1050.46	0.1336	4.33	4.53	17.81	57.97	19.91	N	Flammable, Acute toxic, Environment hazard
Carbonyl Sulfide	2.8	842.76	0.1332	4.84	5.56	11.30	37.23	12.98	N	Flammable, Acute toxic, Irritant, Compressed gas
R11	3.2	227.74	0.1330	9.31	10.68	0.89	4.63	1.34	N	Phased out under Montreal protocol
R141b	3.5	168.04	0.1326	10.84	10.14	0.65	3.71	0.99	N	Banned under Montreal protocol
cis-2-Butene	3.3	311.85	0.1325	7.96	8.68	1.81	8.31	2.44	N	Extremely Flammable, Compressed gas
Dimethyl Ether	3.3	521.68	0.1324	6.15	6.35	5.10	20.10	6.14	N	Flammable

1-Butene	3.5	274.74	0.1321	8.48	6.35	2.55	10.73	3.10	N	Extremely Flammable, Compressed gas
R131I	3.2	442.25	0.1321	6.68	6.62	4.27	16.26	5.15	N	Health hazard, Germ cell mutagenicity
trans-2-Butene	3.4	315.33	0.1318	7.91	8.34	1.99	8.89	2.62	N	Extremely Flammable, Compressed gas
R142b	3.5	333.37	0.1315	7.69	6.64	2.89	12.38	3.55	N	Production is banned under Montreal protocol (Kigali amendment) from January 1, 2020
R1234ze(Z)	3.7	279.34	0.1307	8.41	8.71	1.49	7.61	2.05	Y (A2L safety level)	Lower flammability and toxicity
R152A	3.5	514.55	0.1306	6.19	6.13	5.13	21.05	6.16	N	Extremely Flammable, ODP:0, GWP:124, AL:1.4 years
R1233zd(E)	3.8	209.89	0.1304	9.70	8.63	1.08	5.81	1.50	Y	Non-flammable, ODP:0, GWP:1, AL:0.07123 years
Iso Butene	3.3	382.98	0.1303	7.18	8.24	2.61	11.00	3.38	N	Extremely Flammable, explosive
R123	3.7	189.61	0.1301	10.20	10.05	0.76	4.30	1.14	N	ODP:0.012, GWP:76, Listed in phase out schedule (no more production but can be recycled and used till 2030)
n-Butane	3.5	292.80	0.1301	8.21	7.77	2.08	9.06	2.66	N	Extremely Flammable, Compressed gas
R161	3.3	689.10	0.1291	5.35	5.84	8.05	29.70	9.42	N	Extremely Flammable, Compressed gas, GWP:4

R12	3.2	574.59	0.1290	5.86	6.80	5.66	20.81	6.81	N	Phased out under Montreal protocol
Iso Butane	3.4	358.11	0.1285	7.42	7.25	3.02	12.11	3.74	N	Extremely Flammable, Explosion risk
R245fa	4	255.36	0.1281	8.79	8.86	1.23	6.95	1.74	N	Non-toxic, simple Asphyxiant, ODP:0, GWP:858, AL:7.6 years
R124	3.8	346.67	0.1279	7.55	6.27	3.27	14.13	3.96	N	GWP:527, AL:5.8 years
R245ca	4	203.78	0.1276	9.84	9.62	0.82	5.01	1.23	N	GWP:716, AL:6.2 years
Cyclopentane	3	167.45	0.1272	10.86	14.76	0.35	2.20	0.68	N	Flammable
Diethyl Ether	3.6	184.15	0.1265	10.35	11.49	0.59	3.53	0.96	N	Extremely Flammable, Irritant
R1234ze(E)	3.9	426.35	0.1260	6.80	6.14	4.27	18.01	5.13	Y (A2L safety level)	Lower flammability and toxicity
R1243zf	3.7	477.69	0.1257	6.43	6.19	5.1	19.88	6.06	N	Flammable, Compressed gas
R134a	3.9	554.87	0.1257	5.96	6.08	5.72	23.64	6.83	N	Banned under Montreal protocol
HFE143m	3.8	474.05	0.1256	6.45	6.15	4.95	19.95	5.90	N	Irritant, Compressed gas, explode if heated
n-Propane	3.3	679.18	0.1255	5.39	6.10	8.36	28.49	9.72	N	Flammable
Isopentane	3.3	223.94	0.1255	9.39	11.92	0.77	4.05	1.21	N	Extremely Flammable and Volatile, Irritant, Health and Environment hazard
Neopentane	3.4	267.87	0.1251	8.58	9.44	1.46	6.59	1.99	N	Extremely Flammable, Environment hazard

Propylene	3.3	706.31	0.1251	5.29	5.42	10.17	33.89	11.58	N	Extremely Flammable and Volatile, Environment hazard, Compressed gas
R236EA	4	301.89	0.1250	8.09	8.36	1.72	8.88	2.33	N	GWP:1330, AL:10.7 years
R236FA	4.1	321.56	0.1247	7.83	7.36	2.29	11.09	2.94	N	Compressed gas, Irritant, Asphyxiant
R365MFC	3.9	157.37	0.1233	11.20	11.53	0.46	3.06	0.78	N	GWP:804, AL:8.6 years
R113	3.2	165.50	0.1230	10.92	14.31	0.37	2.32	0.70	N	Phased out under Montreal protocol
Acetone	2.8	181.35	0.1217	10.43	17.40	0.25	1.86	0.61	N	Flammable, Irritant
R1234yf	3.9	576.46	0.1215	5.85	6.64	5.92	22.72	7.07	Y (with proper Air conditioning)	Lightly Flammable
R32	3.9	918.89	0.1210	4.63	4.61	14.75	54.17	16.58	N	Flammable, Compressed gas, ODP:0, GWP:677, AL:4.9 years
R227EA	4.3	400.86	0.1190	7.02	6.40	3.89	16.65	4.69	N	Compressed gas, ODP:0, GWP:3220, AL:31-42 years
RC318	4.1	358.19	0.1171	7.42	7.60	2.66	12.00	3.37	N	Compressed gas, Environment hazard, GWP:10300, AL:3200 years
Methanol	2.8	174.40	0.1167	10.64	19.26	0.13	1.51	0.48	N	Flammable, Acute toxic (oral, dermal, inhalation), Health hazard
R115	4.5	631.57	0.1134	5.59	6.24	7.91	28.22	9.17	N	Phased out under Montreal protocol

n-Hexane	2.9	125.42	0.1127	12.54	18.19	0.16	1.23	0.41	N	Highly Flammable and explosive
Iso hexane	2.8	163.28	0.1127	10.99	18.33	0.23	1.59	0.56	N	Flammable, Hazardous
Novec649	3.9	144.74	0.1036	11.68	13.53	0.33	2.30	0.62	Y	Non-flammable, ODP:0, GWP:1, AL:0.014
Ethanol	2.2	156.95	0.0962	11.21	25.11	0.06	0.88	0.37	N	Flammable
Dichloroethane	1.8	167.87	0.0941	10.84	29.39	0.08	0.77	0.42	N	Flammable, Irritant, Health hazard, Carcinogenicity

Table 5: Fluid list and corresponding parameters for case 1b; ODP & GWP data [47]

Fluid	r_p	P_{sp} (kW / m ²)	Efficiency	D_p (in)	L_{Total} (in)	P_C (bar)	P_B (bar)	$P_{expanded}$ (bar)	Useable?	Reason
Water	20	99.63	0.2485	14.07	3.75	0.02	15.55	0.52	Y	
Acetone	24.6	196.09	0.2413	10.03	3.96	0.25	27.58	1.23	N	Flammable, Irritant
Cyclopentane	19.4	263.74	0.2323	8.65	4.46	0.35	26.47	1.67	N	Flammable
Methanol	20	324.93	0.2323	7.79	4.22	0.13	40.20	1.75	N	Flammable, Acute toxic (oral, dermal, inhalation)
R113	34	156.92	0.2301	11.21	3.60	0.37	27.56	1.15	N	Irritant, banned under Montreal protocol
Ethanol	25	203.29	0.2204	9.85	4.13	0.06	29.81	1.08	N	Flammable
Dichloroethane	13	189.06	0.2187	10.22	4.91	0.08	14.45	1.03	N	Flammable, Irritant, Health hazard, Carcinogenicity
Toluene	20	67.36	0.2149	17.12	4.51	0.03	7.50	0.37	N	Flammable, Irritant, Health hazard, Reproductive toxicity
R141b	19	518.80	0.2115	6.17	5.12	0.65	39.48	3.24	N	Flammable, Potent GHG, ODP - 0.12, GDP - 725, AL - 10 years
Iso hexane	16	335.99	0.1751	7.66	5.64	0.23	21.06	1.91	N	Flammable, Hazardous
n-Hexane	15	286.56	0.175	8.30	5.61	0.16	18.06	1.59	N	Highly flammable and explosive
n-Heptane	10	221.62	0.1456	9.44	6.36	0.05	9.80	1.16	N	Flammable
Ethyl Benzene	5	173.73	0.1272	10.66	7.75	0.01	4.32	0.88	N	Flammable, Irritant
m-Xylene	3	276.87	0.1019	8.44	9.85	0.01	4.09	1.39	N	Flammable, High dose of exposure can cause death

Table 6: Fluid list and corresponding parameters for case 2; ODP & GWP data [47]

Fluid	r_p	P_{sp} (kW / m ²)	Efficiency	D_p (in)	L_{Total} (in)	P_C (bar)	P_B (bar)	$P_{expanded}$ (bar)	Useable?	Reason
Methanol	48	272.33	0.27	8.51	7.24	0.13	40.20	0.67	N	Flammable, Acute toxic (oral, dermal, inhalation)
Cyclopentane	36	258.05	0.2615	8.75	7.21	0.35	26.47	0.86	N	Flammable
Acetone	36	283.33	0.2587	8.35	7.82	0.25	27.58	0.81	N	Flammable, Irritant
R141b	48	284.50	0.2547	8.33	5.93	0.65	39.48	1.22	N	Flammable, Potent GHG, ODP - 0.12, GDP - 725, AL - 10 years
Dichloroethane	25	210.59	0.2523	9.68	9.12	0.08	14.45	0.50	N	Flammable, Irritant, Health hazard, Carcinogenicity
Water	20	249.07	0.2485	8.90	9.38	0.02	15.55	0.52	Y	
R113	45	246.12	0.2413	8.95	7.15	0.37	27.56	0.86	N	Irritant, banned under Montreal protocol
Ethanol	35	344.52	0.2358	7.57	9.17	0.06	29.81	0.75	N	Flammable
Iso hexane	45	217.04	0.2223	9.54	8.10	0.23	21.06	0.66	N	Flammable, Hazardous
Toluene	20	168.41	0.2149	10.83	11.27	0.03	7.50	0.37	N	Flammable, Irritant, Health hazard, Reproductive toxicity
n-Hexane	31	298.66	0.2097	8.13	10.11	0.16	18.06	0.76	N	Highly flammable and explosive
n-Heptane	25	203.49	0.1876	9.85	11.34	0.05	9.80	0.45	N	Flammable
o-Xylene	15	114.10	0.1779	13.15	12.79	0.01	3.62	0.23	N	Flammable, Irritant, Health hazard
n-Octane	20	142.52	0.1643	11.77	12.31	0.01	5.51	0.30	N	Highly flammable, Irritant

m-Xylene	10	198.37	0.1616	9.97	14.71	0.01	4.09	0.41	N	Flammable, High dose of exposure can cause death
Ethyl Benzene	10	210.29	0.1613	9.69	14.74	0.01	4.32	0.43	N	Irritant, Flammable
MM	29.8	176.31	0.1611	10.58	11.29	0.04	9.21	0.40	N	Highly Flammable, Hazardous to aquatic life
n-Nonane	25	63.64	0.1560	17.61	11.51	0.004	3.18	0.13	N	Flammable, Irritant, Health hazard, Environmental hazard
n-Decane	10	95.69	0.1153	14.36	15.24	0.001	1.87	0.19	N	Flammable, Health hazard

Table 7: Fluid list and corresponding parameters for case 2b; ODP & GWP data [47]

Appendix D: Matched steady-unsteady algorithm. Pseudocode

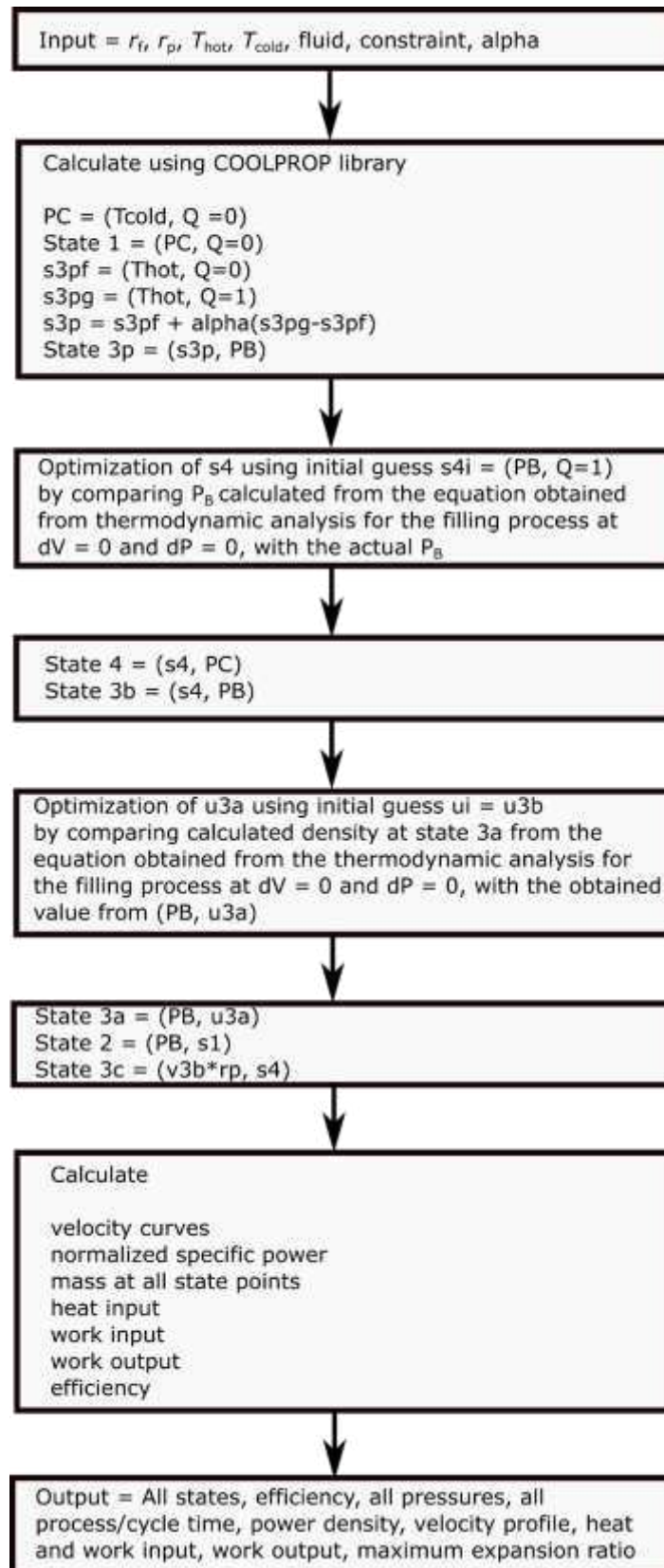


Figure 54: Flowchart to calculate all required parameters for a single fluid based on a given constraint